Hindawi
International Journal of Photoenergy
Volume 2022, Article ID 6009632, 21 pages
https://doi.org/10.1155/2022/6009632

Research Article

An Enhanced P&O MPPT Algorithm for PV Systems with Fast Dynamic and Steady-State Response under Real Irradiance and Temperature Conditions

Ambe Harrison,[1] **Eustace Mbaka Nfah**,[2] **Jean de Dieu Nguimfack Ndongmo**,[3] **and Njimboh Henry Alombah**[4]

[1]*Department of Electrical and Electronics Engineering, College of Technology (COT), University of Buea, P.O. Box Buea 63, Cameroon*
[2]*Department of Electrical and Electronics Engineering, National Higher Polytechnic Institute (NAHPI), University of Bamenda, P.O. Box 39 Bambili, Cameroon*
[3]*Department of Electrical and Power Engineering, Higher Technical Teacher Training College (HTTTC), University of Bamenda, P.O. Box 39 Bambili, Cameroon*
[4]*Department of Electrical and Electronics Engineering, College of Technology, University of Bamenda, P.O. Box 39, Bambili, Cameroon*

Correspondence should be addressed to Ambe Harrison; ambe.harrison@ubuea.cm

Received 20 August 2022; Revised 25 September 2022; Accepted 18 October 2022; Published 8 November 2022

Academic Editor: K. R. Justin Thomas

This paper presents an enhanced perturb and observe (P&O) method for reconciling the trade-off problem between the dynamic response and steady-state oscillations in maximum power point tracking (MPPT). The constraint of having to sacrifice either the dynamic response or the steady-state oscillations has been solved. The method uses the relationship between the open-circuit voltage and maximum power voltage from the fractional open-circuit voltage (FOCV) MPPT method to establish a valid, reduced, and confined search space within which an enhanced P&O via dynamic adaptive step size terminates the search for the maximum power point. The feasibility of the proposed method has been validated by comparing its performance with the conventional P&O algorithm. It was noted that the proposed method increased the operational efficiency of the PV module to 99.89%, reduced the tracking time to 1.8 ms, and preserved the good steady-state response with a power attenuation of less than 0.10 W or relative 0.16% under MATLAB environment. An experimental setup was used to collect real irradiance and temperature data which was used in real-time simulations. The enhanced P&O method was able to resist abrupt changes in irradiance and temperature as it effectively and efficiently followed the maximum power point (MPP). Finally, to appreciate the supremacy of the proposed method, it was compared to nineteen different MPPT methods from literature. The comparison showed that the enhanced P&O MPPT method is highly efficient and effective for MPPT in photovoltaic (PV) generation systems.

1. Introduction

Renewable energy stands as an important springboard to accelerate the world toward a net zero greenhouse gas emissions as we fight against climate change and its dangers. Therefore, a fast transition from fossil fuels, which contributes at least 80% of the world's primary energy to renewable energy, becomes an indispensable step. Solar energy has become an indispensable energy source among other sources. This is due to its cleanliness, abundance, and consistency (US Department of Energy quantifies an hourly 430 quintillion joules of energy from the sun hitting the earth compared to 410 quintillion joules consumed by humans yearly) [1, 2]. The solar cell, which is the building block of photovoltaic (PV) module, has been essential in the conversion of solar energy from the sun into electrical energy [3, 4].

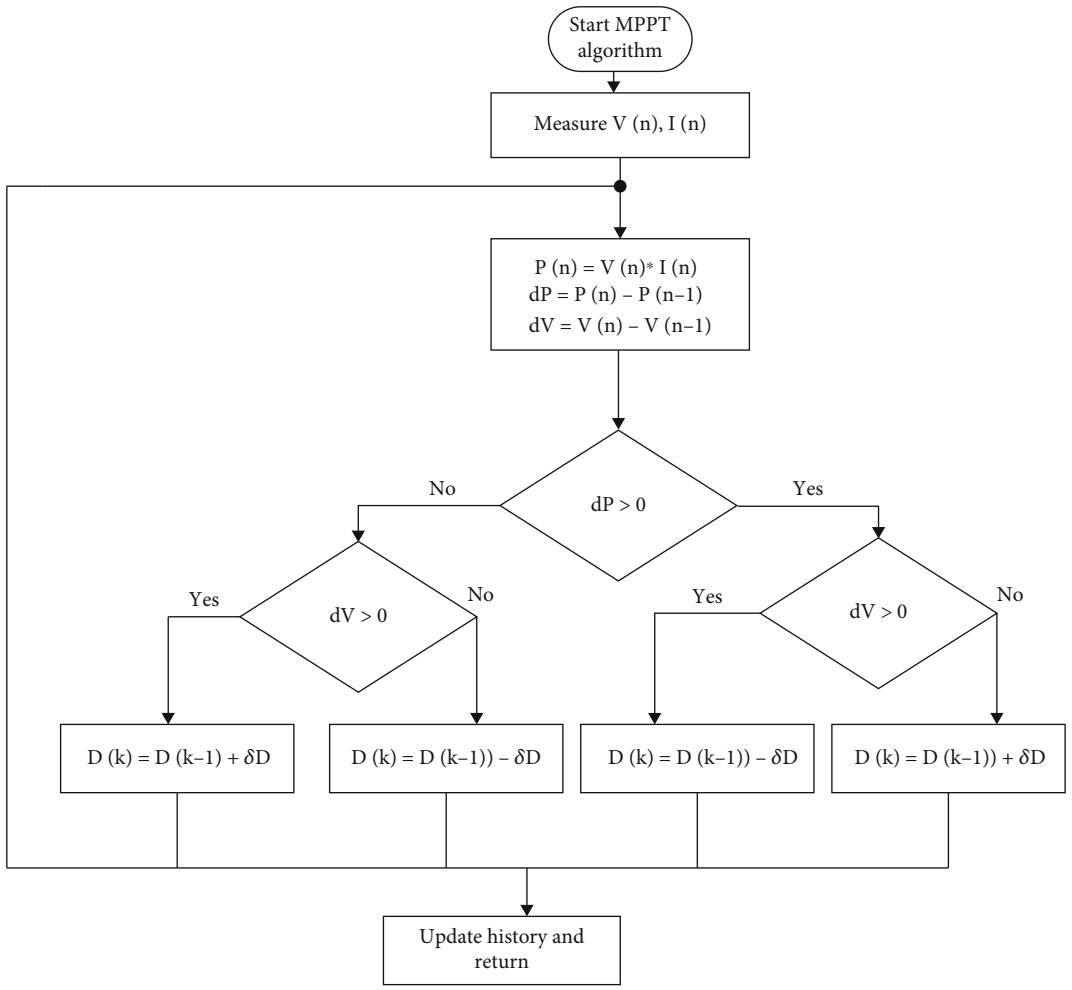

Figure 1: Flowchart of the perturb and observe algorithm [22, 23].

Two objective parameters of the PV module have attracted the attention of researchers during this recent decade: conversion and operational efficiency, the latter being the absolute interest of this paper. The conversion efficiency of commercially available solar panels is very low, limited to 22% [5], with the theoretical limit reaching the possibility of 48.48% [6]. Numerous researches are being done on PV cell design and configuration to optimize the PV cell efficiency [6–10]. Operationally, the PV module is subjected to random environmental conditions such as irradiance and temperature, imposing nonlinearities on the current-voltage characteristics of the PV module. From an energy productivity point of view, the nonlinear behavior implies a nonlinear variation of the delivered power. Therefore, the operational efficiency of a PV module is defined as a measure of how close the actual operating point is to the maximum power point. This operational efficiency is directly related to the cost of installation of the PV system. Considering the very high cost of installation of solar energy systems, a PV module, therefore, has to be operated at maximum efficiency to compensate for its natural cost and this is possible using an MPPT method.

MPPT has attracted the focus of researchers during the recent decades characterized by the deployment of numerous MPPT methods in literature such as fractional open-circuit voltage methods (FOCV) [11, 12], fractional short-circuit current (FSCC) [11, 12], perturb and observe (P&O) [13, 14], Ripple Correlation Control (RCC) [15], system oscillation [16], temperature method [17], current sweep [17, 18], curve fitting method [19], incremental conductance [20], and look-up table method [21]. From the above methods, FOCV and FSCC are the simplest methods for MPPT. However, these methods present serious drawbacks as they require either disconnecting the PV from the load or short-circuiting the PV terminals for a fraction of seconds, a process accompanied by significant energy losses.

P&O has become the most widely used maximum power point algorithm and an inspiration for numerous MPPT methods available in the literature [22, 23]. Perturb and observe algorithm works by disturbing the PV voltage and observing consequent PV power. The P&O is widely installed in commercial inverters and charge controller modules. Despite the popularity of the algorithm, it is greatly challenged by the problem of the trade-off between oscillations at steady-state and dynamic response. The oscillation constraints in the P&O algorithm introduce challenges in the choice of the perturbation parameter. This is because the lower the perturbation size, the lower the oscillations at

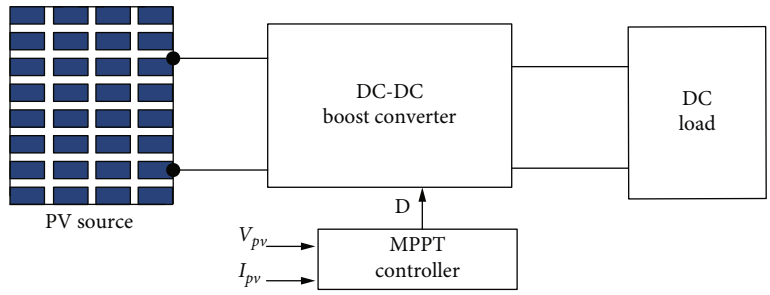

Figure 2: Photovoltaic system made up of PV module, DC/DC Converter, load, and MPPT controller [41].

Table 1: Characteristics of the MSX-60 W solar panel at STC from datasheet.

PV parameter	Value
Maximum power (P_{max})	60 W
Voltage at maximum power (V_{mpp})	17.1 W
Current at maximum power (I_{mpp})	3.5 A
Open-circuit voltage (V_{oc})	21.1 V
Short-circuit current (I_{sc})	3.8 V
Temperature coefficient of V_{oc} (A_v)	-80 mV/°C
Temperature coefficient of I_{sc} (A_i)	0.065%/°C
Number of cells (N_s)	36

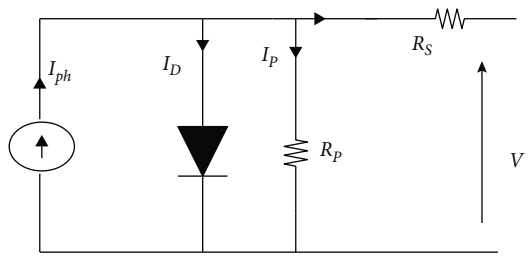

Figure 3: Single-diode equivalent circuit of the solar cell [42].

steady state to the detriment of the dynamic response, unlike a large perturbation parameter that introduces larger oscillations at steady state while increasing the dynamic response. From an energy productivity point of view, oscillation represents energy loss. An alternative to the P&O is the incremental conductance (INC). This method relies on the fact that the derivative of the P-V curve is zero at the maximum power point (MPP). The INC method suffers similar challenges as the P&O: oscillations and tracking inefficiency. However, under certain frequencies, the power extracted by INC is higher than its P&O counterpart [20]. However, when the sampling frequency of the INC is well chosen, the differences in power response time between the INC and P&O are almost negligible [20].

The Ripple Correlation method (RCC) makes use of the power oscillations induced by the inverter to follow the MPP. It uses a high-pass filter to detect and pass power ripples. Based on the derivative of the P-V curve, it determines the operating point of the PV module. Although the RCC method converges faster in tracking the MPP, the initialization time is very low compared to the INC and P&O [11]. The system oscillation MPPT employs a similar methodology as the RCC as they both rely on filters to pass voltage oscillations and estimate the operating point of the PV module. An additional drawback to this method is its mathematical complexity.

The temperature-based method is among the numerous MPPTs available in the literature. works based on the mathematical relationship exiting between the PV module maximum power point voltage and temperature. Although this method is simple and requires only one sensor in computation, it is very inefficient.

The current sweep method is a direct online method. It works by estimating the current-voltage (V-I) curve of the PV and updating it periodically. Although this method follows the maximum power point (MPP), it suffers power loss during the sweeping process; more so, its convergence speed is very slow due to increased complexity. Another less complex MPPT method in literature is the curve fitting method or polynomial approach as found in [19]. This method is inspired by mathematical interpolation. It interpolates the nonlinear characteristics of the PV module offline. Although the method is very simple, it depends on empirical data, which makes the tracking very inefficient. More so, the accuracy of the tracking depends on the order of the polynomial [21].

The above discussed algorithms and methods are challenged by two main problems throughout: dynamic response (speed) and steady-state oscillation that is directly related to power loss from an energy productivity point of view. The aforementioned problems have prompted researchers to look into other alternative solutions to maximum power point tracking.

As an alternative to addressing the dynamic and steady-state constraints of the MPP tracking, Fuzzy logic methods [24], artificial intelligence using artificial neural networks (ANN) [25, 26], and intelligent methods like particle swarm optimization [27], grey wolf optimizer [28], and ant colony have been deployed [29].

The methods of artificial intelligence and fuzzy logic provide satisfactory results in tracking MPP. However, the most important problem of these methods is the conflict between computation load and accuracy. More so, the

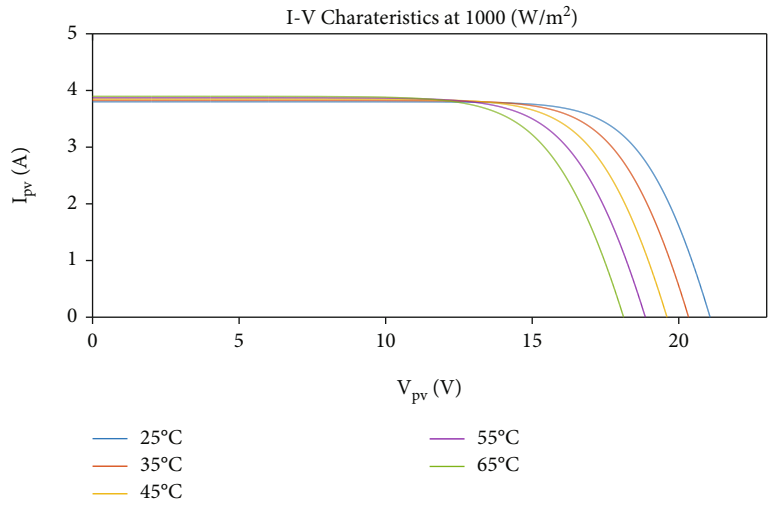

(a)

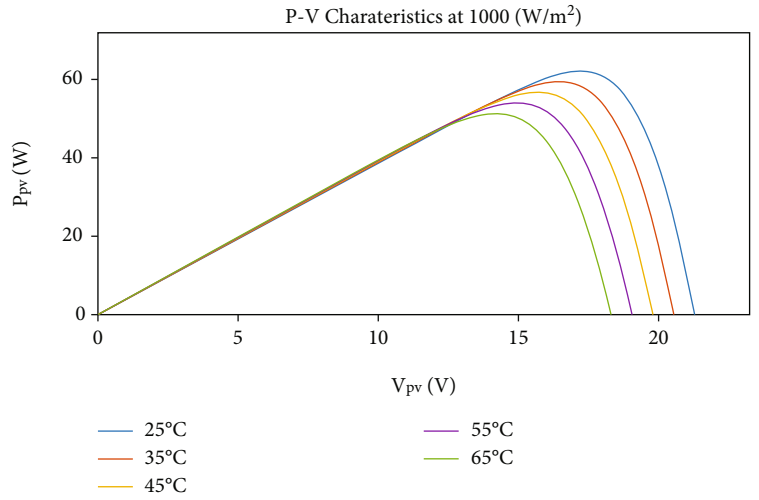

(b)

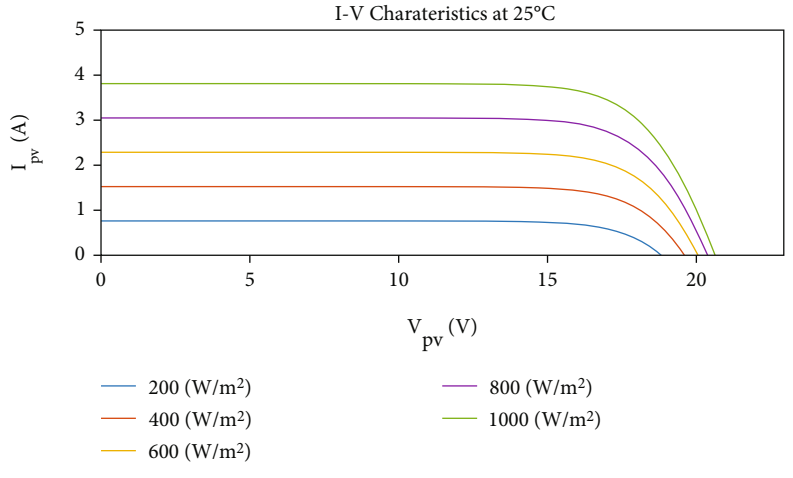

(c)

Figure 4: Continued.

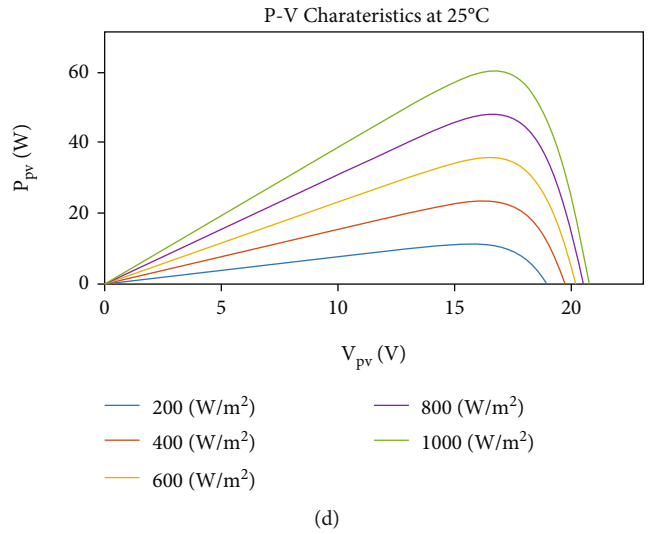

(d)

Figure 4: Current-voltage (a) and power-voltage characteristics (b) (case of constant irradiance and variable temperature) and current-voltage (c) and power-voltage characteristics (d) (case of variable irradiance and constant temperature).

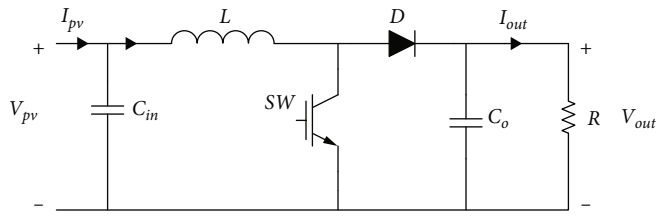

Figure 5: Circuit diagram of the DC-DC boost converter [49].

Table 2: Characteristics of the DC-DC converter.

Converter parameters	Value
Input coupling capacitance (C_{in})	300 μF
Boost inductor (L)	0.3 mH
Switching frequency (F_s)	10 kHz
Boost output capacitance (C_o)	30 μF
Load resistance (R)	10 Ω, 15 Ω

effectiveness of these methods relies on the deep knowledge of the engineer. On the other hand, particle swarms optimization (PSO), grey wolf optimization (GWO), and ant colony optimization (ACO) belong to optimization algorithms. These algorithms are confronted by a similar problem of computational load. Even though they are able to track the MPP with great accuracy, the methods still face low convergence speed.

Therefore, to concretely address maximum power tracking in PV systems, reconciliation must be attained between the dynamic response (tracking speed) and steady-state oscillations.

In a PV grid integrated setting, a self-tuned P&O method [30], learning-based P&O [31], learning-based INC [32, 33], and learning-based hill climbing (HC) MPPT algorithm [34] were developed to concretely address the trade-off problem between steady-state oscillation and dynamic response as well as fixed step size challenges in the P&O, HC, and INC MPPT algorithms. In [30–34], the operating strategy is based on the detection of two conditions, which correspond to the steady-state and dynamic condition when system operation conditions change. Although their method proved to successfully decay the steady-state oscillations in finite time and improved the PV-MPPT system in abrupt changes in irradiance (dynamic conditions), it did not address the transient regime for a given and fixed operating condition, usually characterized by low tracking speed and transient perturbation. Moreover, the complexity and high computational demand of the method are a serious limitation to their method.

The objective in this paper is to develop a simple, less complex, efficient, and enhanced P&O algorithm. The enhanced scheme is considered as a significant assistance to the conventional P&O method such that it tracks the maximum power point at very fast speed while minimizing the oscillations at steady state. The assistance will be inspired fromthe relationship between the open-circuit voltage and the maximum power point voltage. The efficiency and effectiveness of the proposed method will be tested with real-time simulations using measured irradiance and temperature conditions. To show the effectiveness of the proposed enhanced P&O method, its performance will be compared with the conventional P&O and nineteen other different methods in literature.

The rest of the paper is organized as follows: the conventional P&O algorithm is discussed in Section 2. Some modified

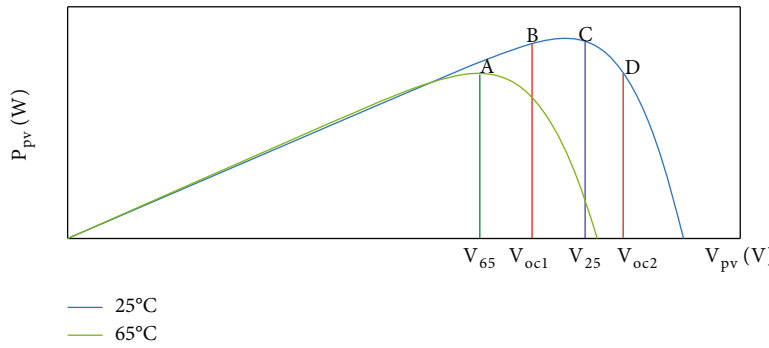

Figure 6: Variation of the MPPT voltage within the search space with variable temperature.

Table 3: Validation of the search space region for MSX-60 W panel.

Temperature (°C)	V_{oc} (V)	V_{mpp} (V)
10	21.28	17.302
20	21.22	17.302
25	21.16	17.302
30	21.1	17.302
35	21.04	16.88
40	20.97	16.88
45	20.91	16.88
50	20.85	16.88
55	20.78	16.88
60	20.71	16.458

Table 4: Estimation of the PV module open-circuit voltage.

Temperature (°C)	10	25	40	60
Current (A)	2.0	1.98	1.96	1.93
Actual V_{oc}	21.28	21.16	20.97	20.71
V_{oc} by Equation (19)	20.37	20.32	20.26	20.19
Relative error (%)	4.28	3.97	3.39	2.5

P&O and INC algorithms from literature are reviewed in Section 3. The PV system and PV cell modelling follow presented in Section 4. Section 5 presents the analysis of the enhanced MPPT. The results of the investigations are presented in Section 6 while the discussions are done in the same section. Finally, the paper is concluded in Section 7.

2. Conventional P&O Algorithm

The P&O MPPT algorithm is the most feasible MPPT algorithm in terms of implementation and incorporation in commercial charge controllers that explains why a special consideration is given to its study in this work. As invoked in the introduction, the P&O and many other derivatives suffer a trade-off between dynamic response (speed) and steady-state oscillations. That is, a sacrifice made between the dynamic response and speed. Three performance parameters will be used to characterize the performance of MPPT algorithm: tracking time (dynamic response), steady-state oscillations, and efficiency. These three parameters form the basis for performance evaluation of MPPT through this paper.

The tracking time constitutes an essential performance evaluation parameter for the MPPT algorithm as defined according to [21], as the time taken by an MPPT algorithm to reach 95% within the maximum average power at MPP.

$$\eta_{\mathrm{MPPT}} = \frac{\int_{t1}^{T} p(t)d(t)}{\int_{0}^{T} p_{\max}(t)d(t)}. \quad (1)$$

The oscillation in this paper is quantified as the peak-to-peak power in watts at steady state, while the efficiency (η_{MPPT}) of the algorithm is the ratio between the area under the power response curve within a specific period of time to the area under the maximum available power over the same period of time as shown in Equation (1) [35].

The flowchart for P&O algorithm is presented in Figure 1. The algorithm measures the PV module current and voltage and consequently the power at every instant. The measured power is compared with the power at the previous instant. Depending on the sign of the change, a linear perturbation displaces the operating point till the maximum power is attained as presented in the flowchart. The performance of the P&O inherently depends on the perturbation size presented as δD in the flowchart. The larger the value of δD, the larger the oscillations at steady state, while the lower the value of δD, the smaller the oscillations and the slower the dynamic response.

3. State of Art Modifications to the Conventional P&O and INC

Many modifications to the conventional P&O and INC algorithm have been proposed in literature. In this section, some of these modifications are discussed while highlighting their shortcomings.

In [36–38], the authors addressed the dynamic-steady state oscillation problematic by proposing a simple dynamic adaptive step size. The fundamental idea of their variable step size is to adjust the step size according to the change in PV power as shown in Equation (2). The fundamental idea of this method is to make large iteration step size during

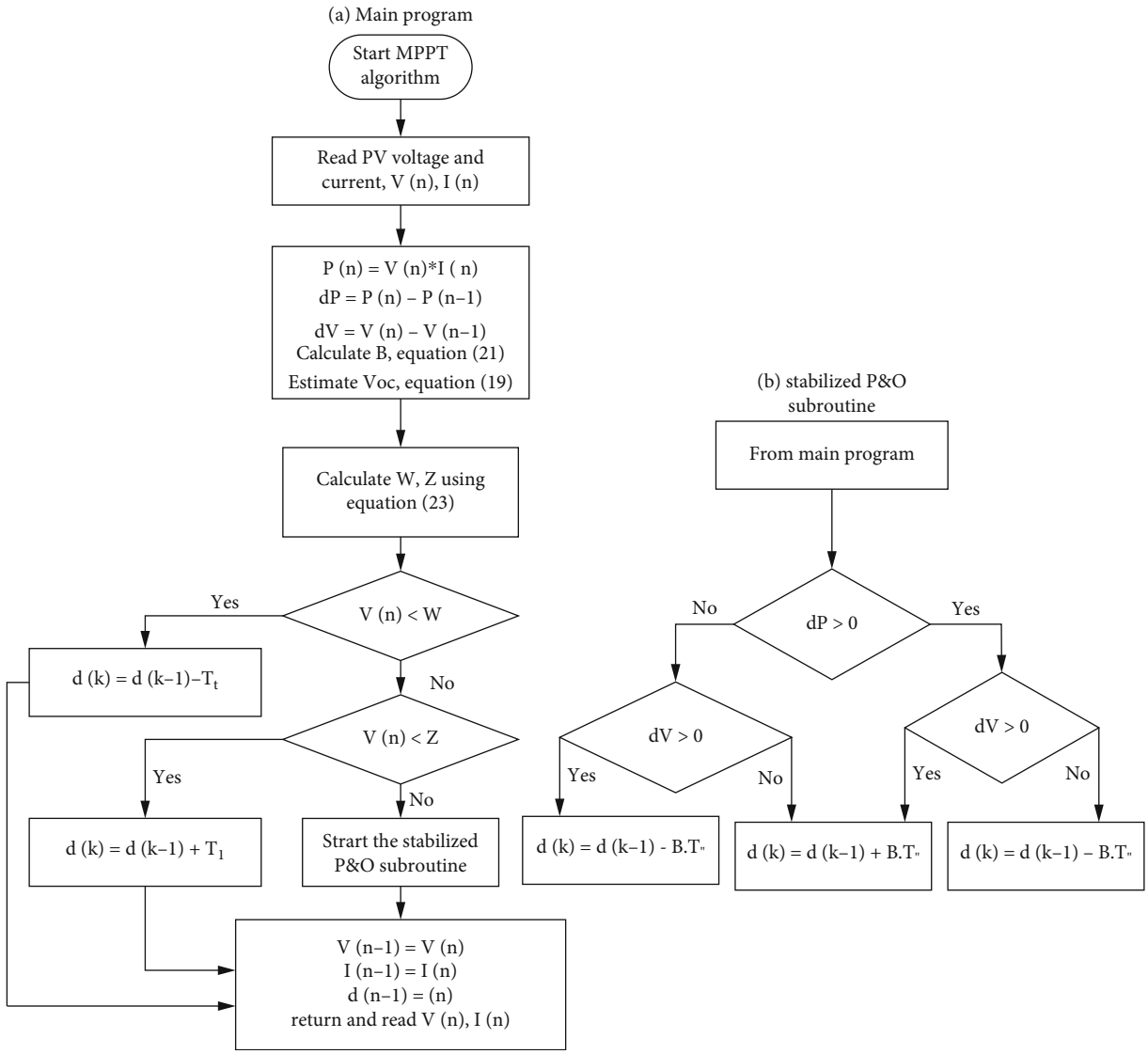

Figure 7: Flowchart of the proposed enhanced P&O algorithm.

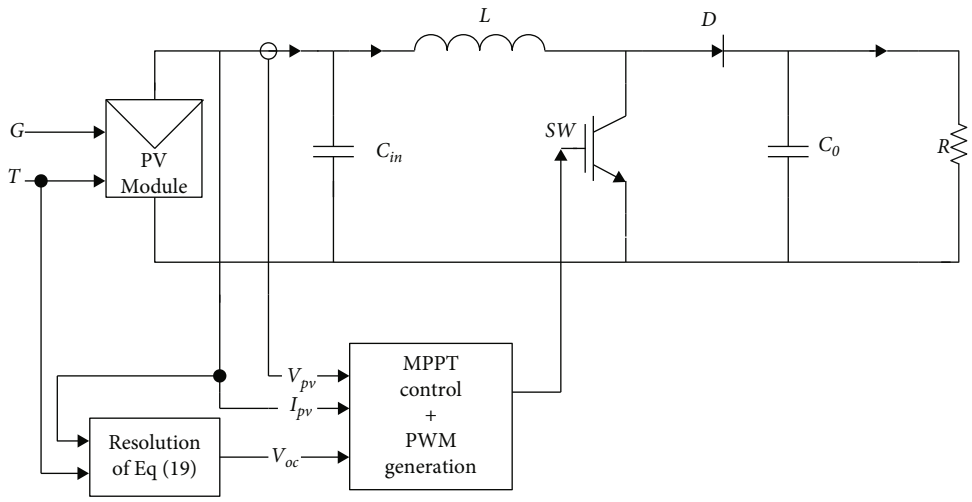

Figure 8: Electrical schematic diagram of the proposed enhanced MPPT.

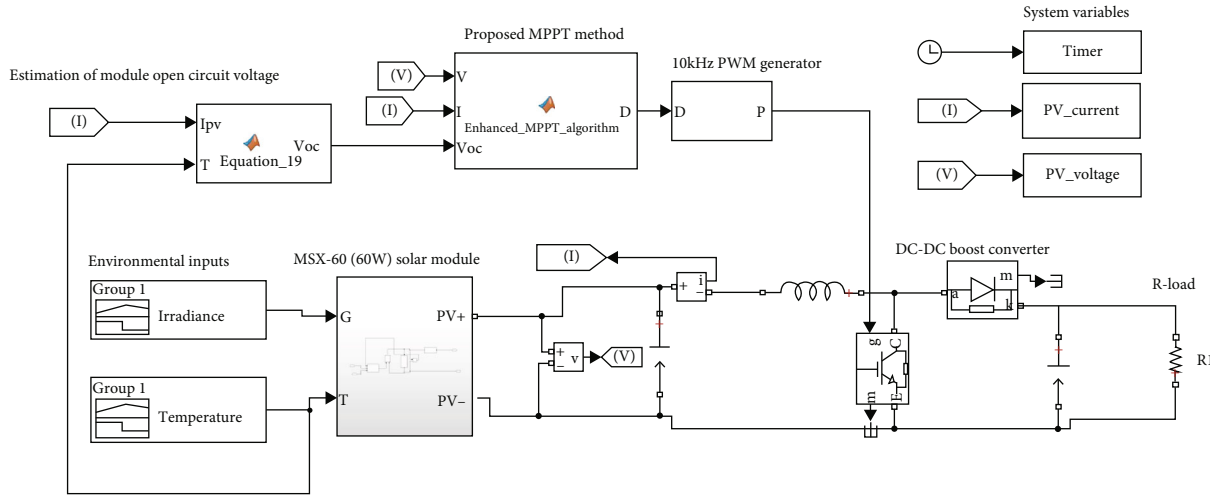

Figure 9: Simulink setup of the proposed enhanced P&O MPPT method.

Table 5: Parameters of the enhanced P&O algorithm.

Parameter	Value
T_1	42%
T_2	0.005%

the transient stage (large change in power) and then a small iteration step size during the steady state when the change in power is relatively small.

$$d(k) = d(k-1) + M\Delta P, \tag{2}$$

where $\Delta P = P(k) - P(k-1)$ is the change in PV module power, $d(k-1)$ is the previous value of the duty cycle, and M is the performance parameter of the adaptation. The modification proposed by [36–38] still leaves behind oscillations at steady state.

In 2004, while addressing the trade-off problematic between the dynamic response and steady-state oscillation, Jain et al. in [39] developed a novel MPPT method based on a new parameter which they called β governed by Equation (3).

$$\beta = \ln\left(\frac{i_{\text{pv}}}{v_{\text{pv}}}\right) - c.V_{\text{PV}}, \tag{3}$$

where $c = q/K.T.n$.

i_{pv} and v_{pv} are the PV module current and voltages, respectively, n is the diode quality factor, and K and T are the Boltzmann constant and temperature. This method calculates two prior parameters $\beta_{\min}$ and $\beta_{\max}$ to determine the boundary between the transient and the steady-state regime. In the transient regime, the error between $\beta_{\min}$ and $\beta_{\max}$ (Equation (4)) tunes the duty cycle, while in the steady-state regime, it is adjusted by any conventional algorithm such as INC or P&O.

$$\begin{aligned} \text{error}\,(e) &= \beta_{\max} - \beta_{\min}, \\ d(k) &= d(k-1) + e \cdot k. \end{aligned} \tag{4}$$

The reliability of the β method makes it one of the most successful approaches in neutralizing the trade-off between dynamic response and oscillations in MPPT. However, its critical drawback lies in its implementation and coordination regarding calculation of the value of β [40]. Moreover, its traceability to the PV module current and voltage complicates the approach [40].

As we raised in the introduction, [30–34] proposed advanced variants of the P&O, INC, and HC while addressing trade-off between steady-state oscillations and dynamic response. Their methods rely on the detection of the steady-state and dynamic condition determined by upper, lu, and lower duty cycle band, ll, whose values are determined at every iteration using Equation (5) and (6):

$$lu = \left(100 + \left(\left(\frac{V_{\text{oc}}}{1 - d_{\text{base}}}\right) - V_{\text{oc}}\right) \times \frac{100}{V_{\text{mpp}}}\right) \times \frac{1}{100}, \tag{5}$$

$$ll = \left(100 + \left(\left(\frac{V_{\text{oc}}}{1 - d_{\text{base}}}\right) - V_{\text{oc}}\right) \times \frac{100}{V_{\text{mpp}}}\right) \times \frac{1}{100}. \tag{6}$$

where V_{oc} is the open-circuit voltage; V_{mpp}, the maximum power voltage; and d_{base}, a based step size, taken as a fixed size of step change in either the conventionally INC, P&O, or the HC. As presented in their different flowcharts, at the beginning of the algorithm, lu and ll are initialized parameters. Equation (5) is a function of the open-circuit voltage; as such, the feasibility and accuracy of lu and ll must depend on the accuracy of the measured or estimated open-circuit voltage. The first obscurity in the works of [30–34] lies in the fact that their method for obtaining the open-circuit voltage was undeclared; as such, it becomes difficult to evaluate the feasibility of their proposed scheme. Moreover, it can as well

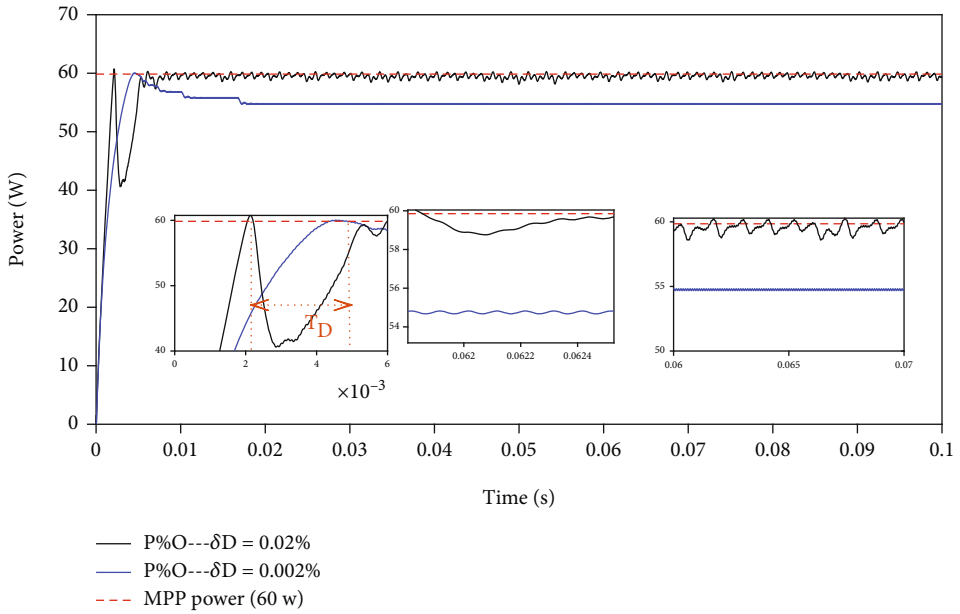

Figure 10: Trade-off illustration with the conventional P&O algorithm.

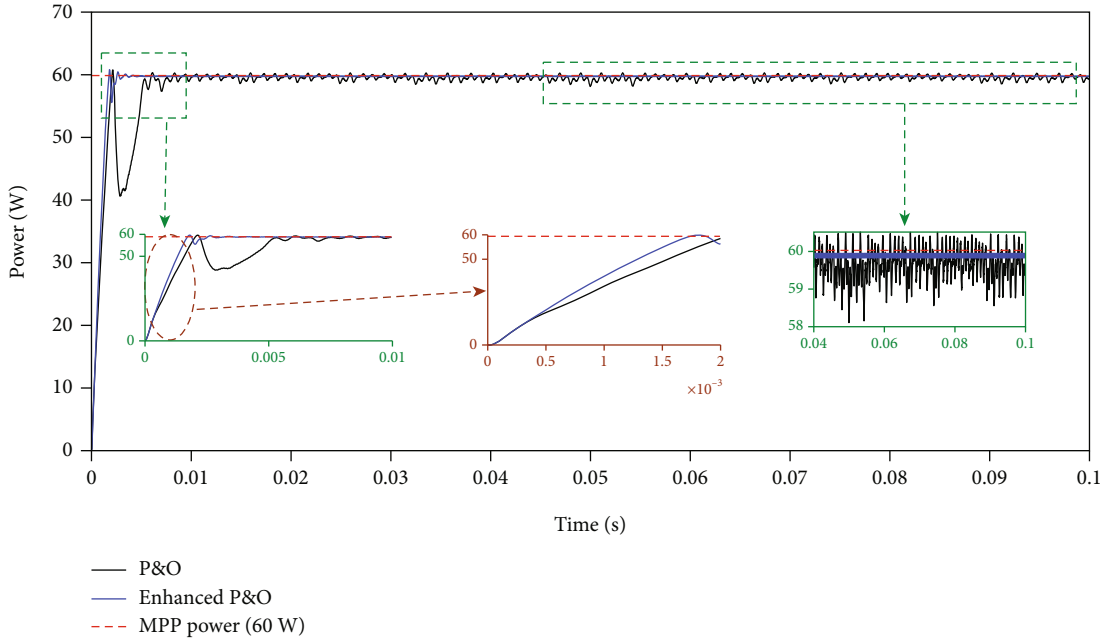

Figure 11: Tracking of MPP power with P&O enhanced P&O method under Test 1.

Table 6: Performance comparison of the enhanced P&O MPPT with the conventional P&O.

MPPT algorithms	Tracking time	Peak-to-peak oscillations	Efficiency
Perturb & observe	2.5 ms	1.5 W (2.5%)	97.90%
Modified P&O	1.8 ms	<0.10 W (0.17%)	99.89%

be seen that both Equations (5) and (6) are functions of the maximum power voltage. The objective of an MPPT algorithm is to drive the PV operating point at the maximum power point at which lies the maximum power voltage. The presence of V_{mpp} in these equations, in addition to the undeclared method for their determination, is a serious limitation to their method. Averagely, from their presented results, a successful decay of the steady-state oscillation and improved dynamic condition were attained, however leaving behind a slow transient response characterized by a tracking time of approximately 0.1 seconds.

In this work, we proposed a method that does not only preserve a feasible, simple MPPT scheme but also one that will resolve the conflicts of trade-off and as well fasten the tracking process in an effective and efficient way. The clarity

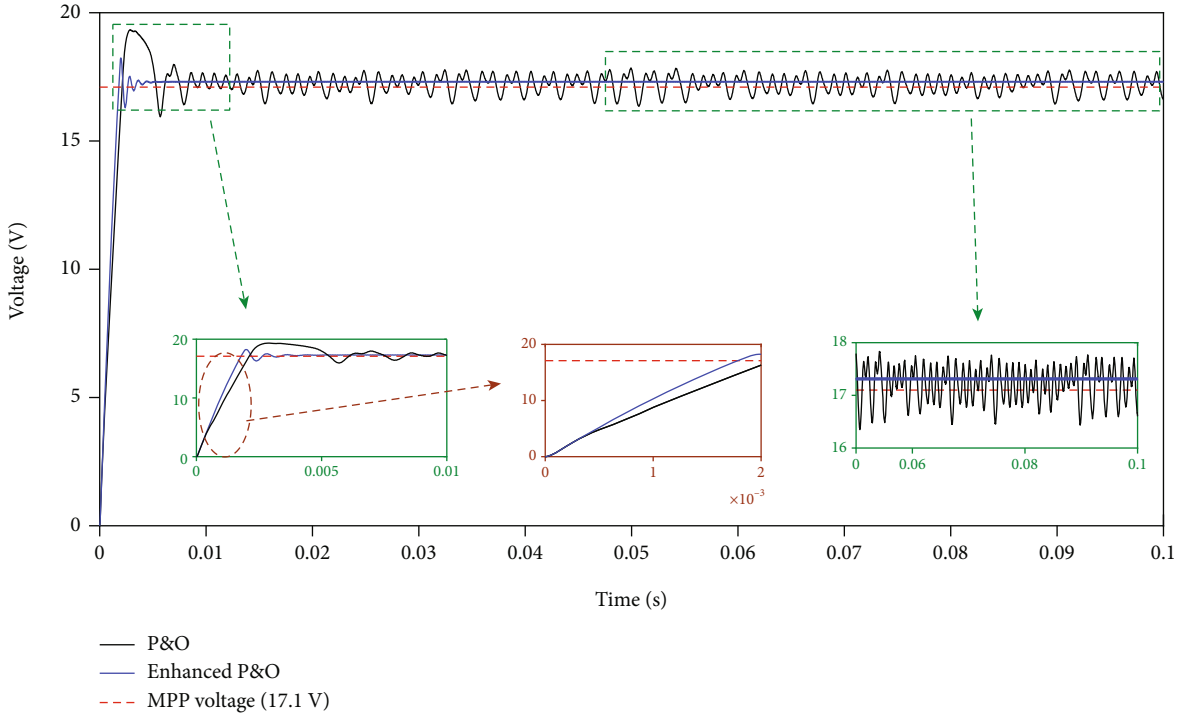

Figure 12: Tracking of MPP voltage with P&O enhanced P&O method under Test 1.

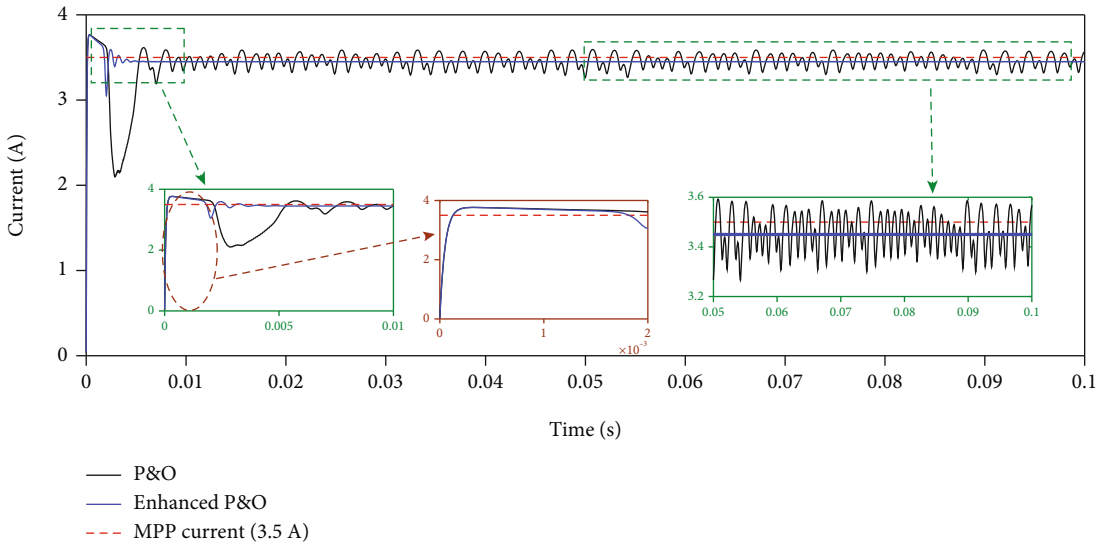

Figure 13: Tracking of MPP current with P&O and enhanced P&O MPPT method under Test 1.

of the work and the estimations of open-circuit voltage are well presented and justified.

4. PV System Model

Figure 2 shows the basic topology of a photovoltaic (PV) system. It consists of a DC/DC converter, load, PV module, and the MPPT control unit.

4.1. Modelling of PV Cell. Operationally, the PV module is exposed to random variations of environmental parameters such as irradiance and temperature. Manufacturers of solar panels only make available functional parameter such as open-circuit V_{oc}, short-circuit current I_{sc}, voltage at MPP V_{mpp}, current at MPP I_{mpp}, the temperature coefficients of open-circuit voltage, and short-circuit current, A_v and A_i, respectively. In addition, these parameters are only available under standard test conditions (STC), 1000 W/m^2 and 25°C. To accurately design the proposed enhanced method, a detailed study of the PV module is carried out under diverse atmospheric conditions.

In this paper, MSX-60 W is selected as the PV module of consideration. Its electrical characteristics at STC from datasheet are presented in Table 1.

The solar cell is the basic building block of a solar module. A typical module is an assembly of solar cells. Due to its accuracy, the single-diode model has been widely used to model the solar cell as reported in [43–48]. In this work, the single mode shown in Figure 3 is adopted for this study. The model consists of an ideal current source (I_{ph}), in parallel with a diode (D) and a shunt resistor (R_s) forming a series network with a series resistor (R_p). The current source supplies current in response to solar irradiance (G) which is also a function of temperature (T). The diode models are the semiconductor. The mathematical equations for the PV cell model are presented in Equations (7)–(13) [42].

$$I = I_{ph} - I_D - I_p, \tag{7}$$

$$I_p = \frac{V + I.Rs}{R_p}, \tag{8}$$

$$I_D = I_S\left[\exp\left(\frac{V + I.R_s}{nV_T}\right) - 1\right], \tag{9}$$

where I_D is the diode current, I_{ph} is the photocurrent, I_p is the shunt resistor, V_T is the thermal voltage, V is the cell output voltage, I_s is the diode saturation current, and n is the nonlinearity factor of the diode. The thermal voltage depends on temperature and can be written as

$$V_T = \frac{K_B T}{q}, \tag{10}$$

where T represents the actual cell temperature in kelvin T_{ref}, the temperature at STC; K_B is the Boltzmann constant with value 1.381×10^{-23} J/K; q is the electron charge with fundamental value 1.602×10^{-19} C; and E_g is the semiconductor's bandgap energy.

The short-circuit current being inherently dependent on the irradiance G is written as

$$I_{ph} = [I_{scr} - A_i(T - T_i)]\frac{G}{1000}, \tag{11}$$

where I_{scr} is te reference short-circuit current at STC and G is the solar irradiance in watt per square meter. Moreover, the saturation current (I_s) is written in terms of the short-circuit current and the open-circuit voltage as follows:

$$I_s = I_{s\_ref}\left(\frac{T}{T_{ref}}\right)^3 e^{\left[\left(qE_g/nK_B\right)\left((1/T_{ref})-(1/T)\right)\right]}, \tag{12}$$

where I_{s_ref} is the reference saturation current.

Combining the above equations results in the mother equation governing the characteristics of the solar cell as presented in the following equation:

$$I = I_{ph} - I_S\left[\exp\left(\frac{V + I.R_s}{nV_T}\right) - 1\right] - \frac{V + I.R_s}{R_p}. \tag{13}$$

The characteristic graph obtained in Figure 4 is based on the mathematical equations of the PV cell. I-V and P-V curves for variable temperature between 25 and 65°C at fixed irradiance of 1000 W/m^2 are presented in Figures 4(a) and 4(b). Intuitively, it can be seen that despite the nonlinear characteristics, there exists a point on the curve where there is maximum available power. More so, the graph shows that variation in temperature affects the position of the MPP point. Figures 4(c) and 4(d) show the characteristics of the same PV module under variable irradiance in the range 200-1000 W/m^2 at a fixed temperature of 25°C. The four graphs in Figure 4 indicate that the maximum power point (MPP) varies with both changes in temperature and irradiance, respectively.

4.2. DC-DC Boost Converter. The boost converter is a DC-DC step-up converter. From an energy point of view, it is used to control the transfer of energy from the PV module to the load at high efficiency. Figure 5 shows the circuit diagram of the boost converter. It constitutes capacitor C_{in} and inductor L, a transistor SW, an ouput capacitor C_o, and a load R. V_{pv}, I_{pv}, I_{out}, and V_{out} are the PV current, voltage, output current, and voltage. Consider an ideal boost converter such that the power input (P_{in}) equal to the power output P_{out}, and their representation in terms of current and voltage is written mathematically as

$$P_{in} = P_{out}, \tag{14}$$

$$I_{pv}V_{pv} = I_{out}V_{out}. \tag{15}$$

At steady state, the following equation holds for the converter

$$V_{pv} = (1 - d)V_{out}. \tag{16}$$

The resistance seen by the PV module is formulated based on Equations (15) and (16):

$$R_{pv} = (1 - d)^2 \cdot R. \tag{17}$$

The boost converter represents an impedance emulator, modifying the resistance seen by the PV according to the duty cycle (d) of the switching signal as shown in Equation (17). This equation is the basis for voltage variation in maximum power point tracking algorithm. The parameters of the converter are chosen such that the converter operates in continuous conduction mode (CCM). These parameters are presented in Table 2.

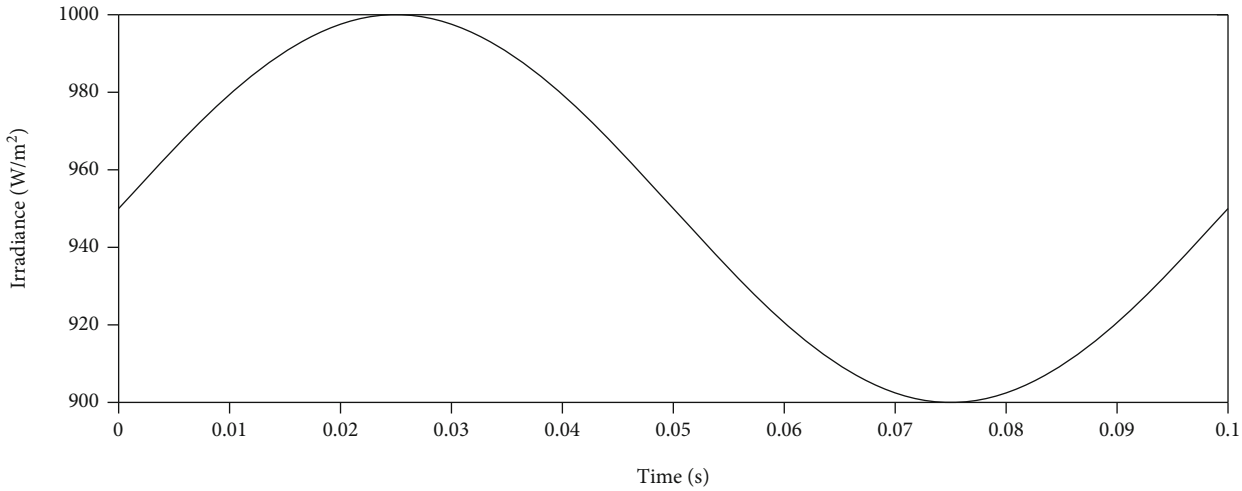

Figure 14: Sinusoidal variation of solar irradiance.

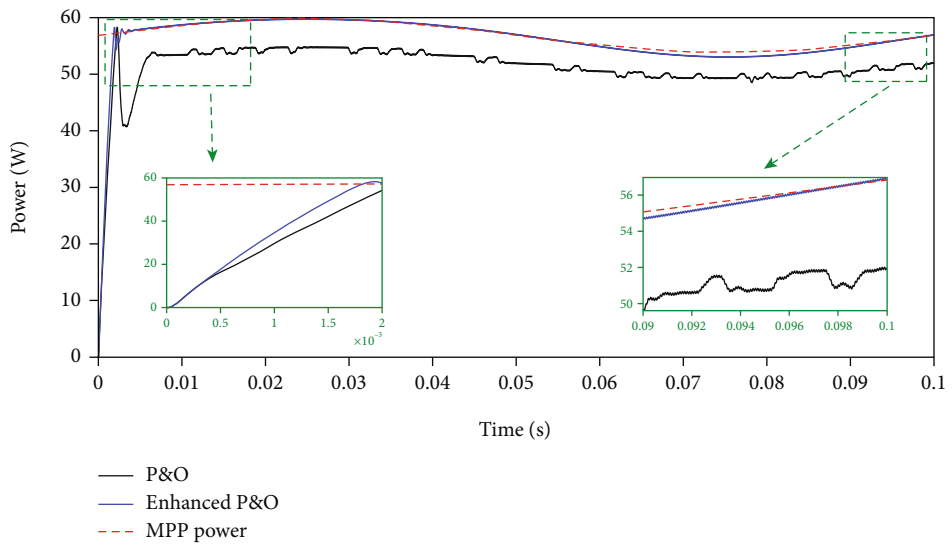

Figure 15: Tracking of MPP power with P&O, ideal MPPT, and enhanced P&O MPPT method under Test 2.

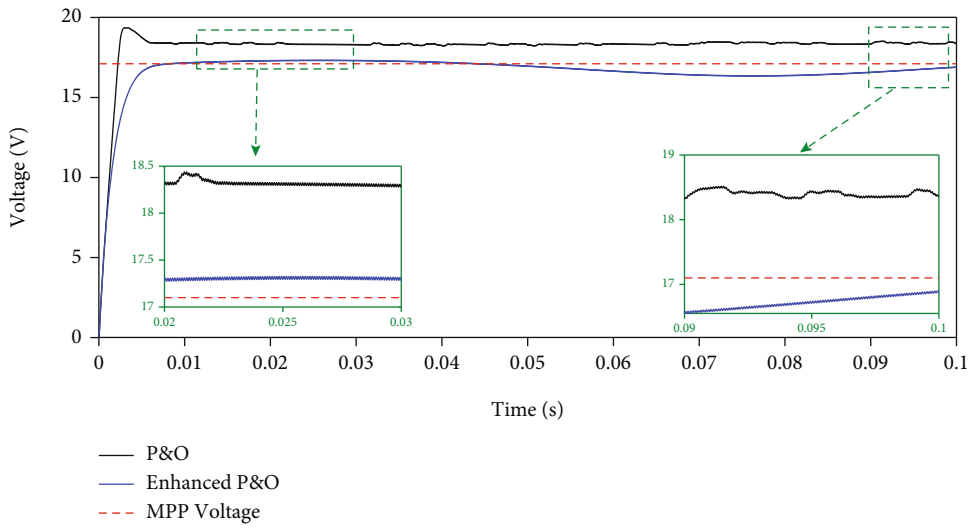

Figure 16: Tracking of MPP voltage with P&O and enhanced P&O MPPT method under Test 2.

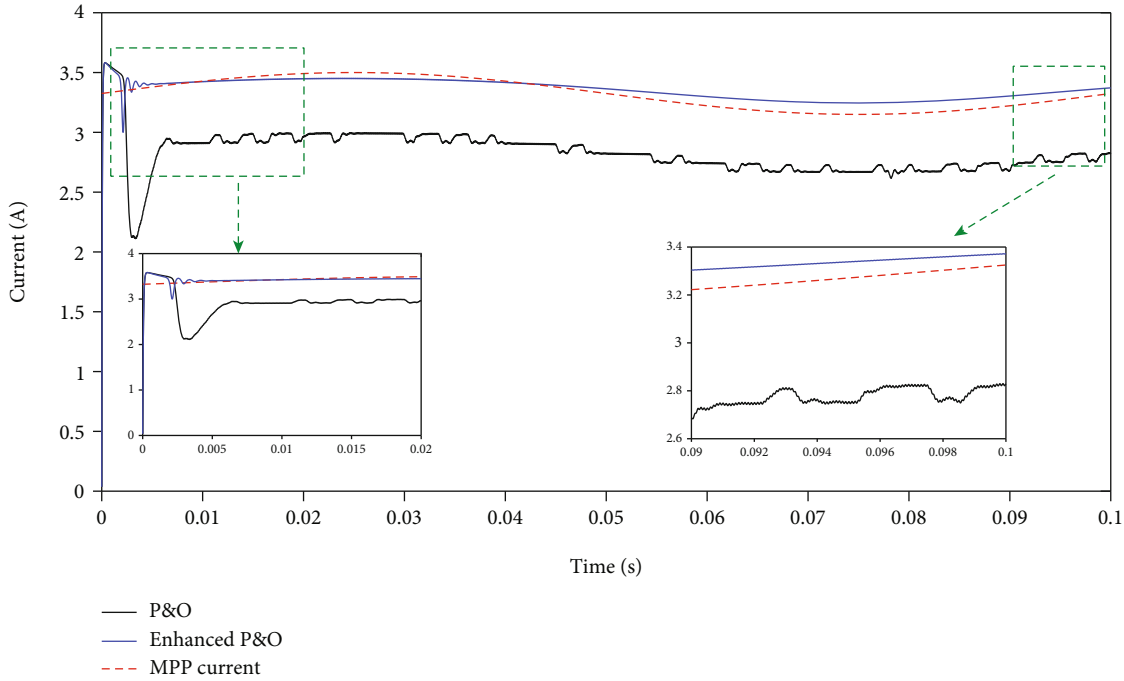

Figure 17: Tracking of MPP current with P&O and enhanced MPPT method under Test 2.

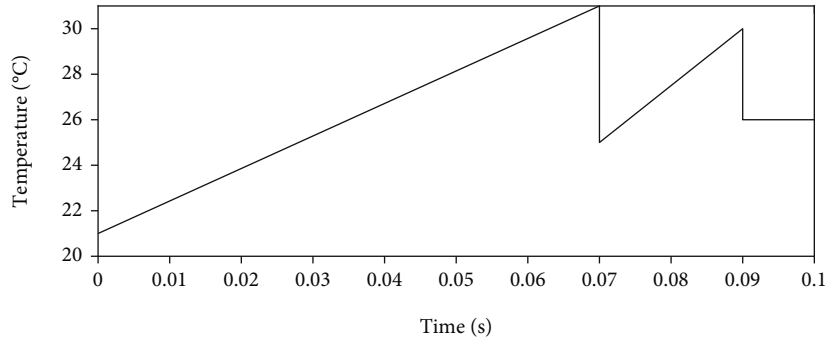

Figure 18: Temperature conditions for Test 3.

5. Analysis of the Enhanced MPPT Method

The proposed enhanced P&O algorithm is analyzed in two descriptive steps: search space confinement and stabilized perturb and observe algorithm.

5.1. Search Space Confinement. The dynamic response of the P&O MPPT algorithm depends inherently on the search space. In this study, the relationship between the open-circuit voltage and maximum power point voltage (Equation (18)) from the FOCV method defines the confined valid search space.

$$V_{\text{mppt}} = K_{\text{pv}} V_{\text{oc}}, \quad K_{\text{pv}} \in [0.8\ 0.9], \tag{18}$$

where K_{pv} is a numeric value in the range $K_{\text{pv}} \in [0.8\ 0.9]$, according to [50].

By mathematical intuition, if K_{pv} is limited by the open-circuit voltage established in Equation (18), we demonstrate by simulation that the maximum power voltage must be found in the vicinity of this region set by K_{pv}, that is, V_{oc1} and V_{oc2} as presented graphically in Figure 6. V_{oc1} and V_{oc2} are the lower and upper confined limits, respectively, of the maximum power point voltage set by K_{pv}. V_{65} and V_{25} are considered the respective MPP voltage at 65°C and 25°C, respectively. The idea of search space confinement was randomly invoked and used by [51]. However, the authors failed to elaborate the description behind the search space confinement as they randomly choose and set a search space region. In this paper, the choice of the search space is defined by the relationship between the open-circuit voltage and maximum power point voltage. Moreover, we give a serious consideration to the variability of search space in order to always guarantee that the algorithm does not track the wrong MPP point.

The graphical schematic to elaborate the variability of the MPP voltage with temperature within the search region is presented in Figure 6. Considering the blue P-V curve to

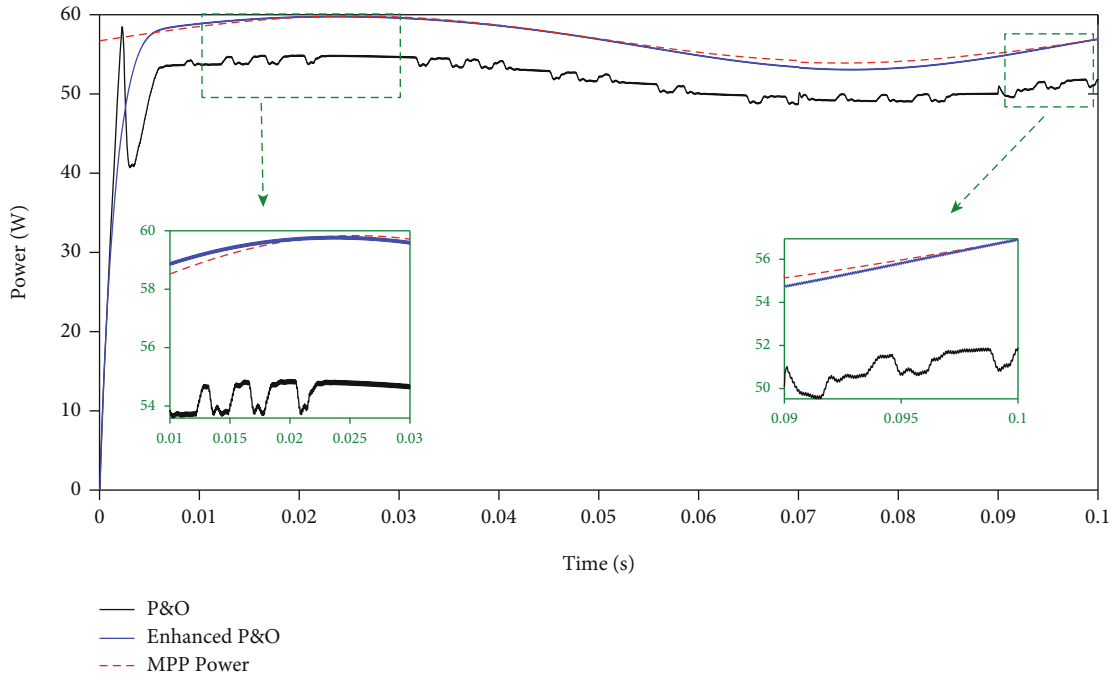

Figure 19: Tracking of MPP power with P&O and enhanced P&O MPPT method under Test 3.

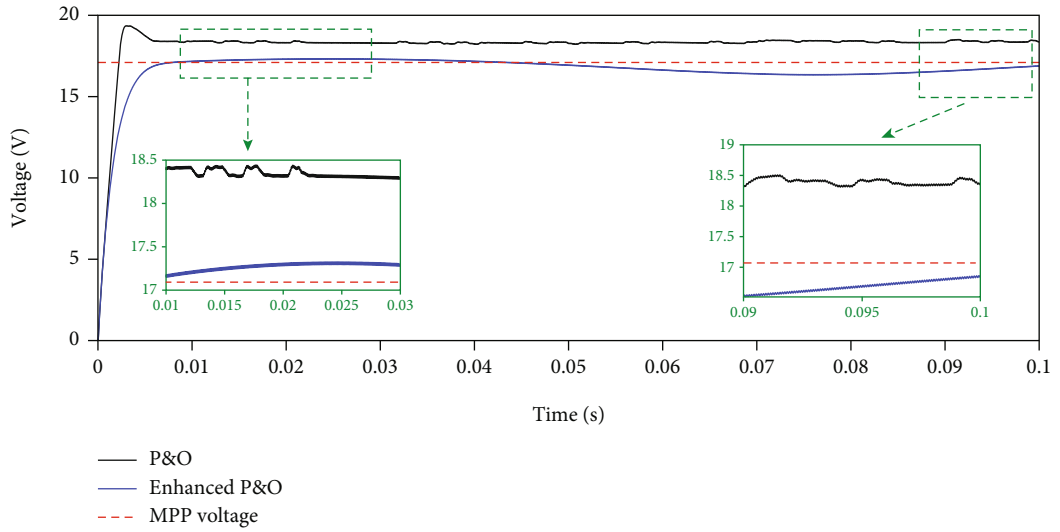

Figure 20: Tracking of MPP voltage with P&O and enhanced P&O MPPT method under Test 3.

represent the PV characteristic at 25°C, at 25°C, the MPP is at C, where the MPP voltage V_{25} lies. Following the search space in Equation (18), V_{oc1} and V_{oc2} establish the search region, [B-D]. In addition, considering that in another instant, temperature increases from 25°C to 65°C, under this new operating temperature, the new P-V characteristics become the green curve presented in Figure 6, with its maximum power point at A. If the previous search space [B-D] will not change because of this increase in temperature, the MPPT algorithm will track a wrong maximum power a serious problem that was not considered in [51]. This problem will be very critical in conditions characterized by large and rapid changes in temperature because the algorithm will experience large drifts, slowing its response and contributing to energy losses.

To get rid of this problem, a mechanism that enables the confined search space to change following variations in temperature must be introduced. In this paper, the dynamics of the confined search space is ensured by estimation of the PV module open-circuit voltage at every cycle of the algorithm. Firstly, to confirm that the MPP voltage will always lie in the vicinity of the confined search space, investigations are

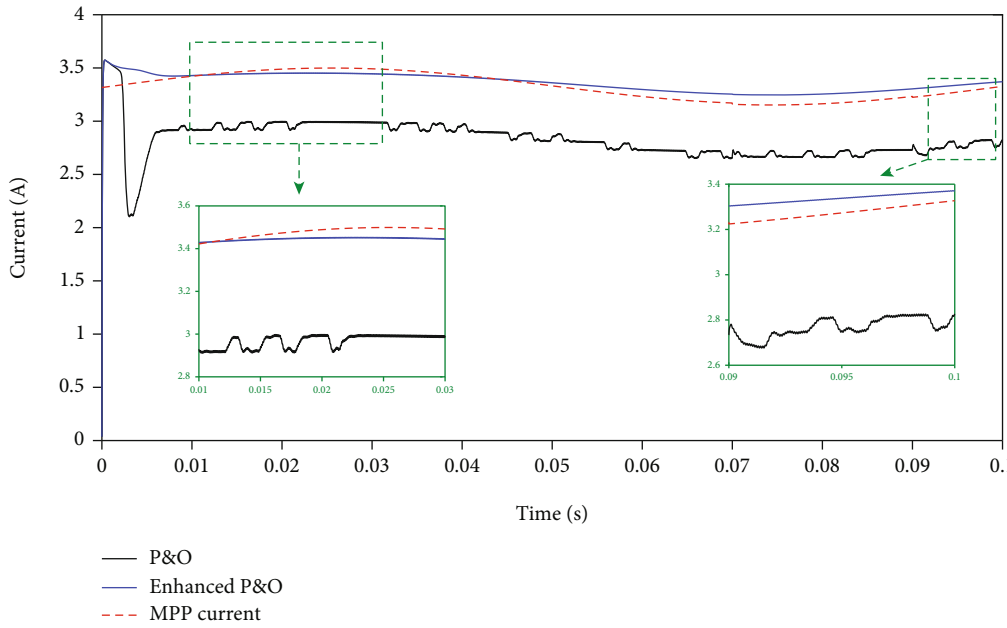

Figure 21: Tracking of current with P&O and enhanced P&O MPPT method under Test 3.

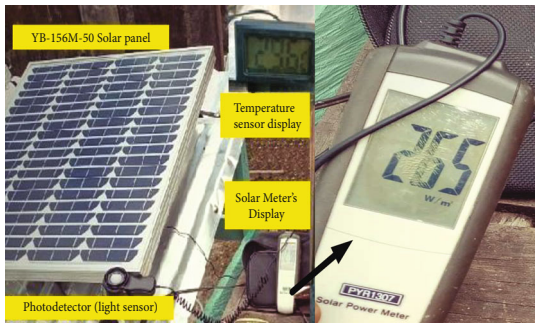

Figure 22: Experimental setup for real-time data collection.

carried out with the MSX-60 W solar module whose characteristics are presented in Table 1. As presented in Table 3, it is found that the MPP voltage lies within 75-85% of the open-circuit voltage. Moreover, it can be seen from the same table that this range is preserved even under worst temperature and irradiation conditions. Therefore, the said range is adopted in this paper. However, for all practical and experimental purpose, the range 75-90% can always guarantee that the maximum power voltage lies in the search region.

The open-circuit voltage was estimated using Equation (19) as reported in [51].

$$V_{oc} = V_{oc\_STC} + nV_t \ln\left(\frac{I_{PV}}{I_{SC-STC} + A_i(T - T_{STC})}\right) + A_V(T - T_{STC}), \tag{19}$$

where G_{STC}, V_{oc_STC}, and T_{STC} are the solar irradiance, open-circuit voltage, and temperature at reference (STC). These parameters are directly obtained from the datasheet. $n, A_v, A_i\, T$, and G are the diode ideality factor, temperature coefficient of open-circuit voltage, temperature coefficient of short-circuit current, PV temperature, and irradiance, respectively.

The estimated values of the open-circuit voltage according to Equation (19) under different variations of temperature are presented in Table 4. The empirical values are close to the actual values. However, under extreme conditions, Equation (19) introduces a relative error of 4.28%, as presented in Table 4. The relative error is less than 5%, which is acceptable and satisfactory for a PV module. From a speed of response point of view, the presented search space confinement method can guarantee an enhanced P&O algorithm. However, to simultaneously enhance the steady state, by reducing the oscillations, a stabilized routine is introduced. The stabilized routine comes in to solve the trade-off problematic between dynamic response and steady state.

5.2. Stabilized P&O Subroutine. Once the confined search region is established, the P&O is further enhanced via a stabilized routine in order to terminate the search for maximum power. The adaptive step size that ensures stabilization is presented in the following equation:

$$d(k) = d(k-1) \pm B \cdot T_2, \tag{20}$$

$$B = \frac{dV}{\sqrt{dP^2 + dV^2}}, \tag{21}$$

where T_2 is the stabilization step size (predifined constant) and B the dynamic adaptive parameter. A good choice of T_2 ensures that the steady oscillations are minimized. This paper does not provide an exact approach to estimate T_2. However, it was found from simulations and trials that Equation (23) is a realistic guide for choosing the value of

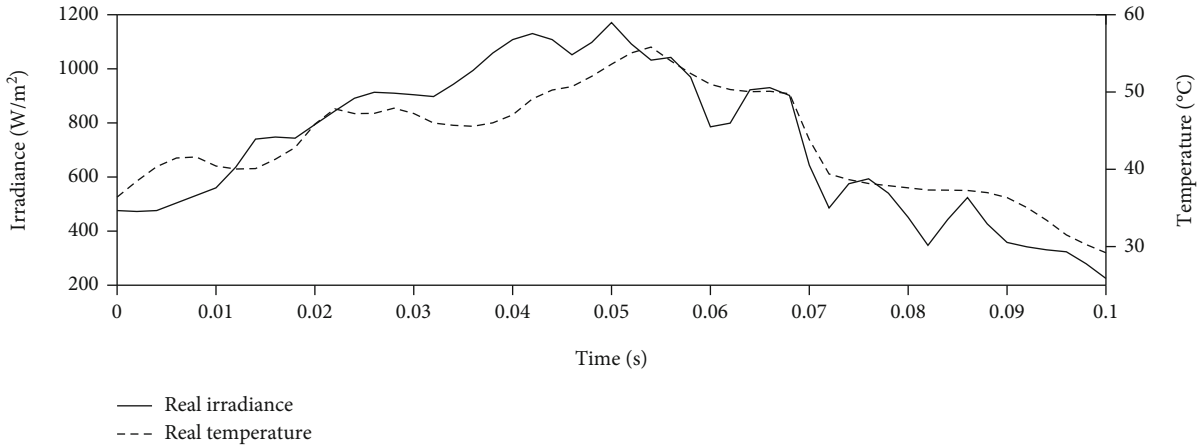

Figure 23: Real-time irradiance and temperature.

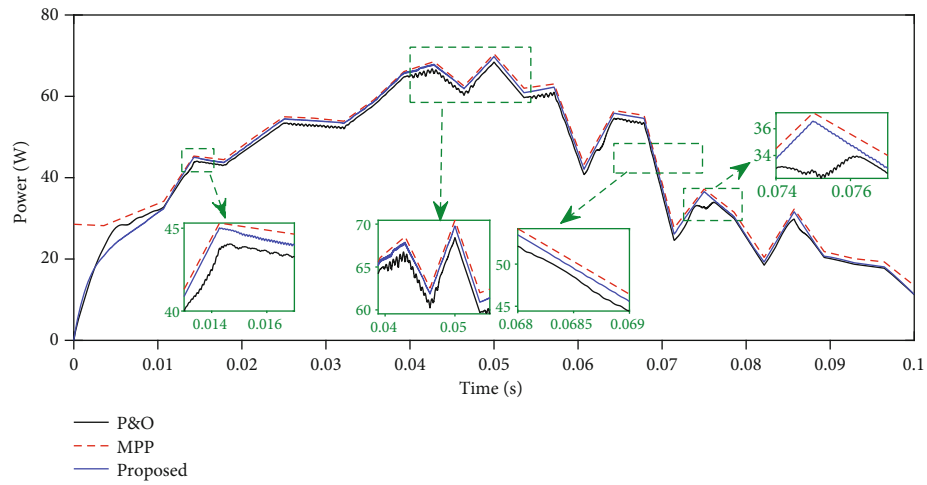

Figure 24: Tracking of the real-time condition maximum power with the P&O and the enhanced MPPT algorithm.

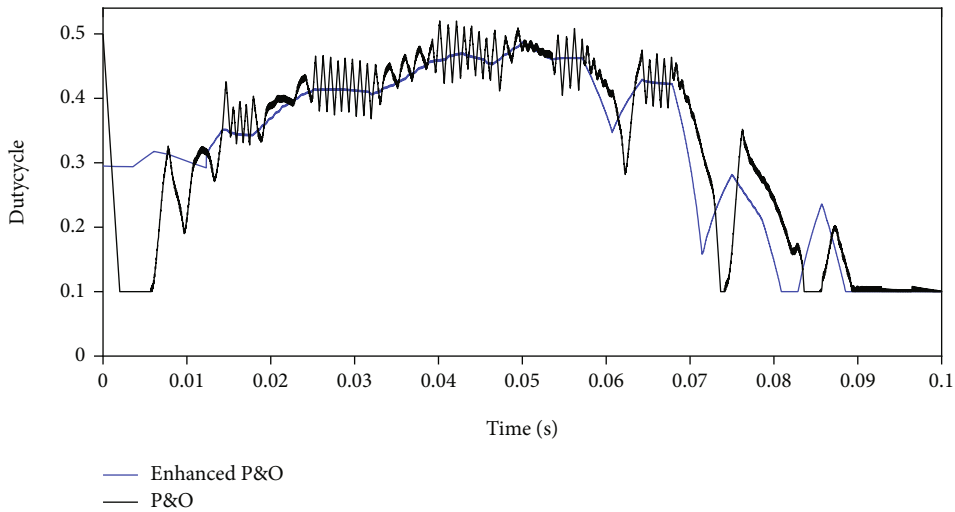

Figure 25: Duty-cycle control according to the P&O and the enhanced P&O MPPT under real condition.

Table 7: Comparison of the enhanced MPPT algorithm with other MPPT methods in literature at STC.

Ref	Year	DC-DC converter type	MPPT algorithm	Tracking time (ms)	Oscillations (W)	Efficiency (%)
[51]	2021	Boost	Novel MPPT tactic	9.6	x	99.86
[53]	2022	Boost	Innovative MPPT	10	x	99.75
[54]	2021	Boost	Thermal imaging-based P&O	0.22	x	x
[55]	2018	Boost	Variable universe fuzzy logic	x	x	x
[56]	2022	Boost	Modified P&O	18	x	99.80
[57]	2019	Boost	Modified P&O	13	x	x
[58]	2016	Boost	Improved beta	500	x	x
[59]	2015	Buck-boost	Improved P&O	x	x	99.4
[60]	2018	Boost	Modified P&O	9	x	x
[61]	2021	Boost	Modified variable INC	12.6	1.6 (0.8%)	99.73
[62]	2008	Boost	Variable INC	120.3	3.3	99.45
[63]	2016	Boost	Variable INC	18.4	2.1 (1.5%)	99.65
[64]	2017	Boost	Variable INC	27.3	2.8 (1.86%)	99.53
[65]	2014	Buck	INC	2.5	2.7 (3.4%)	98.8
[66]	2013	Boost	PI controller-based P&O	20	20 (10%)	95%
[67]	2012	Buck	Fuzzy-based P&O	1500	2 (1.3%)	98.5
[68]	2014	Boost	Adaptive P&O-fuzzy	20	1 (0.5%)	95.1
[69]	2014	X	TS fuzzy-based INC	2000	1 (2.5%)	97.5
[70]	2011	Buck	Load current-based MPPT	80	0.04 (0.4%)	97
Proposed	—	Boost	Modified P&O	1.8	0.1 (0.17%)	99.89

T_2. In Equation (23), T_1 is the acceleration step size used by the search space confinement routine .

Considering the search space region and Equation (19), we have

$$\left.\begin{aligned} W &= V_{OC1} = 0.75V_{OC} \\ Z &= V_{OC2} = 0.85V_{OC} \end{aligned}\right\}, \tag{22}$$

$$T_1 \gg T_2, \tag{23}$$

where W and Z are the lower and upper bound of the confined search space.

In Figure 7, the flowchart of the novel algorithm is presented shown as a combination of search space confinement and stabilized P&O subroutine. The algorithm computes the PV module voltage, current, and power with the corresponding estimation of the open-circuit voltage. If the actual voltage is lower than the lower bound of the search space (W), the duty cycle is decreased, controlled by T_1, to increase the PV module voltage until the condition is satisfied. An increase of duty cycle occurs when the PV module voltage is instead greater than the upper bound (Z) such that the PV voltage is reduced and driven into the search region. Once the operating point lies within the search region, a variable step size as shown in Equations (20) and (21), respectively, is used to terminate the search for the MPP point. Therefore, in the proposed method, the temperature is sensed and uses for the computation of the open-circuit voltage according to Equation (19). Globally, the enhanced MPPT method receives the estimated open-circuit voltage, PV module current, and voltage, respectively, and runs the algorithm as presented in the flowchart of Figure 7, to control the gate of the transistor as shown schematicaly in Figure 8.

The Simulink setup for the proposed enhanced P&O is presented in Figure 9, while its parameters are displayed in Table 5, respectively.

6. Results and Discussions

The performance of the proposed enhanced P&O has been tested within the MATLAB/Simulink environment via numerical simulations with a sample time of 1 μs. A simulation time of 0.1 s was considered for both virtual and real-time variations of irradiance and temperature. The MATLAB Simulink setup is presented in Figure 9. For every simulation, the maximum power point (MPP) variable is presented. They have been represented in red dotted lines for all the figures. These variables, MPP current and voltages, have been estimated mathematically as functions of the operating conditions, G and T, according to [52]. Though the method is an approximation, the objective was to have a primary MPP reference.

The various simulations carried are divided into three main subsections. Illustration of the trade-off problematic in conventional P&O is presented in Subsection 6.1. In Subsection 6.2, the enhanced P&O MPPT is compared with the conventional P&O under various conditions of virtual temperature and irradiance. The performance of the proposed method is validated in Subsection 6.3, via real-time simulation. Finally, the efficiency and the enhanced MPPT are compared with 19 other methods in the literature.

6.1. Trade-Off Problematic in the Conventional P&O. To demonstrate the dynamic response and trade-off problem in the conventional P&O, two distinct perturbation sizes were used to control the switching signal of the conventional P&O algorithm as presented in Figure 10. When the step size perturbation is varied (reduced) from 0.02% to 0.002%, it was calculated that the tracking time reduced (T_D) by 2 ms while the oscillation dropped from 1.5 W to 0.15 W, reducing the efficiency from 97.89 to 90.90%. Intuitively, the relatively smaller the step size perturbation of0.002%, reduced the steady-state oscillation but sacrificed the dynamic speed, a serious problem that this paper addresses. This variation in the MPPT performance parameters is critical, it may be perceived as very small values in magnitude. However, its consideration becomes very fundamental when the PV system contains an array of modules operating at relatively high orders of power. In this work, special consideration is given to reduce the steady-state oscillations to a negligible value, accelerating the dynamic speed while boosting the PV system efficiency.

6.1.1. Standard Test Conditions (Test 1). In this test termed Test 1, simulations are carried out under standard test conditions (STC). At STC, the solar module's maximum power, voltage, and current are depicted on datasheet or Table 1, 60 W, 17.1 V, and 3.5 A. The results are compared with the conventional perturb and observe algorithm. From Figure 11, it can be seen that the proposed enhanced MPPT method increases the dynamic response while almost suppressing the steady-state oscillations. The performance comparisons of the two algorithms are further presented in Table 6. The enhanced P&O increases the tracking efficiency of the MPPT from 97.90% to 99.89% while reducing the tracking time to 1.8 ms. The power oscillations of 1.5 W peak to peak sustained in the conventional P&O are reduced to almost zero (<0.1 W) in the proposed MPPT, hence validating the conflict resolution between dynamic response and steady-state oscillation.

It is worth noting that the enhanced P&O leaves a steady-state offset or deviation in voltage by 0.2 V as could be seen in Figure 12 and 0.14 A of steady-state current offset, Figure 13. These deviations are reflected in the power curve of Figure 11, as a small drop in the steady-state power by 0.07 W was recorded. These deviations are relatively small values and almost negligible, principally because the efficiency of the PV system remained very high.

Furthermore, it can be seen from the voltage tracking curves in Figure 12 that the P&O introduces large oscillations at steady state unlike the enhanced P&O; the oscillations are reduced cancelled to almost zero. This observation can be further confirmed in Figure 13, in which the corresponding current tracking curve is presented, an almost zero steady-state oscillation for the enhanced scheme while the P&O continues to oscillate at steady state.

Therefore, the supremacy of the enhanced MPPT is obvious as it preserves the tracking stability of the PV system by following the MPP voltage and current unlike the conventional P&O that showed large oscillations even with the best choice of the perturbation parameter.

6.1.2. Sinusoidal Irradiance Test (Test 2). In the second test, termed Test 2, the P&O and enhanced P&O MPPT algorithms are exposed to sinusoidal variations in irradiance and fixed temperature (25 degrees Celsius) as presented in Figure 14.

The main objective of the sinusoidal test is to demonstrate the effectiveness of the enhanced MPPT compared with conventional P&O under sinusoidal increasing and decreasing irradiance.

In Figure 15, it can be seen that the enhanced MPPT algorithm follows the MPP under sinusoidal irradiance conditions. On the other hand, the P&O gets stuck and lacks behind the MPP. In terms of dynamic response, it can be seen that the enhanced MPPT is faster than the conventional P&O. Under this dynamic condition, the enhanced MPPT reconciles the dynamic response (speed) and steady-state oscillation. From Figure 16, magnifying the potion of the voltage curve between the time instant, 0.09 to 1 s, it is seen that the enhanced P&O follows the MPP voltage in an increasing manner. It can also be confirmedin the same figure that during this same span, the P&O exhibits large steady deviation from the MPP voltage, a natural problem of the conventional P&O that has been termed "Drift" in the literature of MPPT.

A similar drifting can be perceived in the current tracking curve in Figure 17, within the time span 0.09 to 0.1 s. Under this same span, it can be seen the enhanced P&O continuously follows the MPP current.

6.1.3. Sinusoidal Irradiance and Variable Temperature (Test 3). In the last test, termed Test 3, the algorithms are investigated based on their potential to follow the MPP power under sinusoidal changing irradiance as is presented in Figure 14 as well as variable temperature as shown in Figure 18. Figure 18 is a blend of both slowly changing temperature and rapidly changing temperature. The justification for simulation under both changing irradiance and temperature lies in the fact that faced to practical conditions, environmental parameters(temperature and irradiance) are not constant. Therefore, simulations under dynamic conditions give a better evaluation of the MPPT algorithm. To that end, the objective of Test 3 is to see and appreciate the extent to which the algorithms can resist both changes in irradiance according to a sinusoidal profile and fast and slowly changing temperatures.

When the P&O and enhanced P&O are subjected to both variable irradiance and temperature, firstly, it can be seen in Figure 19 that the proposed enhanced P&O continues to seek for the MPP while the conventional P&O continues to lack behind. Magnifying the region of the curves between 0.08 and 0.1 seconds shows that the enhanced P&O is void of oscillations as opposed to the P&O that sustains large oscillations. The drift problem is further seen from the potion of the curve 0.09 s to 0.1 s. The P&O completely lost the tracking direction. From the same figure, it can be seen that the enhanced P&O is a significant assistance to the conventional P&O as it is able to solve the drift problem.

In Figure 20, a similar condition of drift away from the MPP voltage can be perceived for the P&O algorithm.

Furthermore, magnifying the region between 0.01 s and 0.03 s shows that the P&O does only loss direction but oscillates as well. Although the enhanced P&O shows minor deviations, it continues to seek for the MPP. A similar scenario can be observed in Figure 21.

Figures 19–21 validate that the enhanced P&O is not only superior to the conventional P&O but can also withstand abrupt changes in temperatures and irradiance conditions, as it effectively follows the MPP under this conditions.

6.2. Response to Real Irradiation and Temperature Conditions. An experimental setup was mounted in the site of the University of Buea to collect real irradiation and temperature on site. Data were collected at intervals of 15 minutes, from 9:30 am-4 pm on 25/02/2022, which is a period of the dry season in the site location, University of Buea, Cameroon. The daily data was used to generate a signal of 29 data points spaced between 0 and 0.1 s to represent the time period of 9:30 am-4 pm. The experimental setup consisted of a sample solar panel, PYR1307 pyrometer for irradiance measurement, and a digital thermometer based on LM35 temperature sensor for temperature measurement on the PV panel. The experimental setup to achieve the aforementioned data collection is presented in Figure 22.

The collected solar irradiance and temperature are presented as curves in Figure 23. The proposed algorithm is subjected to the real operating conditions in Figure 23. The result of the simulations under the aforementioned conditions for power tracking is presented in Figure 24. It can be seen in the same figure that both the P&O algorithm and the enhanced P&O MPPT follow the maximum power point (MPP) as presented in red on the graph. However, the enhanced MPPT tracks the MPP more efficiently than the P&O. Moreover, under real conditions, it is seen that the P&O sustains power oscillations, a drawback which is almost reduced to zero in the enhanced MPPT scheme.

The evolution of the duty cycle for the P&O and the proposed enhanced MPPT under real irradiance and temperature is presented in Figure 25. It can be seen in this figure that the proposed MPPT greatly improves the dynamic behavior of the PV system, hence validating the conflictresolution between dynamic response and steady-state oscillations.

To appreciate and generalize the performance of the proposed enhanced P&O MPPT algorithm, it is compared with 19 available MPPT algorithms in the literature as shown in Table 7. From a comparative point of view, it can be seen that the enhanced P&O MPPT algorithm is superior to the available MPPT methods in literature.

7. Conclusion

In this paper, an enhanced P&O MPPT algorithm for PV systems has been presented. The enhanced method uses the relationship between open-circuit voltage and maximum power voltage from fractional open-circuit voltage to set a reduced and confined valid search space, within which an enhanced P&O using dynamic adaptive step size terminates the search for the maximum power point. Simulation results under virtual environmental conditions generated in MATLAB as well as in real conditions proved the feasibility of the proposed method. Moreover, the proposed method resolved the conflict of trade-off between steady-state oscillations and dynamic response, suffered by the classical INC and P&O. Finally, the proposed method is compared to 19 other MPPT methods from the literature. Averagely, the enhanced MPPT method proved to significantly increase the efficiency of the PV system.

Data Availability

All data used to support the findings of this study are included within the paper.

Conflicts of Interest

The authors declare that they have no conflicts of interest.

References

[1] W. Chen, Y. Duan, L. Guo, Y. Xuan, and X. Yang, "Modeling and prediction of radiated emission from solar cell in a photovoltaic generation system," *IEEE Journal of Photovoltaics*, vol. 6, no. 2, pp. 540–545, 2016.

[2] A. D. Mills and R. H. Wiser, "Changes in the economic value of photovoltaic generation at high penetration levels: a pilot case study of California," *IEEE Journal of Photovoltaics*, vol. 3, no. 4, pp. 1394–1402, 2013.

[3] M. Le Feuvre and M. A. Wieczorek, "Nonuniform cratering of the Moon and a revised crater chronology of the inner Solar System," *Icarus*, vol. 214, no. 1, pp. 1–20, 2011.

[4] S. Sajadian and R. Ahmadi, "Distributed maximum power point tracking using model predictive control for photovoltaic energy harvesting architectures based on cascaded power optimizers," *IEEE Journal of Photovoltaics*, vol. 7, no. 3, pp. 849–857, 2017.

[5] C. G. Popovici, S. V. Hudişteanu, T. D. Mateescu, and N.-C. Cherecheș, "Efficiency improvement of photovoltaic panels by using air cooled heat sinks," *Energy Procedia*, vol. 85, pp. 425–432, 2016.

[6] F. H. Alharbi and S. Kais, "Theoretical limits of photovoltaics efficiency and possible improvements by intuitive approaches learned from photosynthesis and quantum coherence," *Renewable and Sustainable Energy Reviews*, vol. 43, pp. 1073–1089, 2015.

[7] S. Bhattacharya and S. John, "Beyond 30% conversion efficiency in silicon solar cells: a numerical demonstration," *Scientific Reports*, vol. 9, no. 1, p. 12482, 2019.

[8] W. Farooq, A. D. Khan, A. D. Khan, and M. Noman, "Enhancing the power conversion efficiency of organic solar cells," *Optik*, vol. 208, article 164093, 2020.

[9] K. Saraswat, "Luminescence efficiency enhancement for different solar cells designs," *International Journal of Advanced Trends in Computer Science and Engineering*, vol. 9, no. 2, pp. 2043–2048, 2020.

[10] A. Torbatinezhad, A. A. Ranjbar, M. Rahimi, and M. Gorzin, "A new hybrid heatsink design for enhancement of PV cells performance," *Energy Reports*, vol. 8, no. 6, pp. 6764–6778, 2022.

[11] P. Bhatagar and R. K. Nema, "Maximum power point tracking control techniques: state-of-the-art in photovoltaic

applications," *Renewable and Sustanaible Energy Reviews*, vol. 23, pp. 224–241, 2013.

[12] A. R. Reisi, M. H. Moradi, and S. Jamasb, "Classification and comparison of maximum power point tracking techniques for photovoltaic system: a review," *Renewable and Sustainable Energy Reviews*, vol. 19, pp. 433–443, 2013.

[13] F. Liu, Y. Kang, Y. Zhang, and S. Duan, "Comparison of p& o and hill climbing mppt methods for grid-connected pv converter," in *2008 3rd IEEE Conference on Industrial Electronics and Applications*, pp. 804–807, Singapore, 2008.

[14] N. Femia, G. Petrone, G. Spagnuolo, and M. Vitelli, "Optimization of perturb and observe maximum power point tracking method," *IEEE transactions on power electronics*, vol. 20, no. 4, pp. 963–973, 2005.

[15] M. A. Eltawil and Z. Zhao, "MPPT techniques for Photovoltaic applications," *Renewable and Sustainable Energy Review*, vol. 25, pp. 793–813, 2013.

[16] S. Jaim and V. Agarwal, "Comparison of the performance of maximum power point tracking schemes applied to single-stage grid-connected photovoltaic systems," *IET Electric Power Applications*, vol. 1, no. 5, pp. 753–762, 2007.

[17] J. Ramos-Hernanz, I. Uriarte, J. M. Lopez-Guede, U. Fernandez-Gamiz, A. Mesanza, and E. Zulueta, "Temperature based maximum power point tracking for photovoltaic modules," *Scientific Reports*, vol. 10, no. 1, 2020.

[18] B. Subuhi and R. Pradhan, "A comparative study on maximum power point tracking techniques for photovoltaic power systems," *IEEE Transactions on Sustainable Energy*, vol. 4, no. 1, pp. 89–98, 2013.

[19] D. Verma, S. Nema, A. M. Shandilya, and S. K. Dash, "Maximum power point tracking (MPPT) techniques: Recapitulation in solar photovoltaic systems," *Renewable and Sustainable Energy Review*, vol. 54, pp. 1018–1034, 2016.

[20] I. Houssamo, F. Locment, and M. Sechilariu, "Maximum power tracking for photovoltaic power system: development and experimental comparison of two algorithms," *Renewable Energy*, vol. 35, no. 10, pp. 2381–2387, 2010.

[21] S. Agarwal and M. Jamil, "A comparison of photovoltaic maximum power point technques," in *2015 annual IEEE India conference (INDICON)*, pp. 1–6, New Delhi, India, December 2015.

[22] L. Piegari and R. Rizzo, "Adaptive perturb and observe algorithm for photovoltaic maximum power point tracking," *IET Renewable Power Generation*, vol. 4, no. 4, pp. 317–328, 2010.

[23] E. Mamarelis, G. Petrone, and G. Spagnuolo, "A two-steps algorithm improving the P&O steady state MPPT efficiency," *Applied Energy*, vol. 113, pp. 414–421, 2014.

[24] L. K. Narwat and J. Dhillon, "Design and operation of fuzzy logic based MPPT controller under uncertain condition," *Journal of Physics: Conference Series*, vol. 1854, no. 1, article 012035, 2021.

[25] F. Sedaghati, A. Nahavandi, M. A. Badamchizadeh, S. Ghaemi, and M. Abedinpour Fallah, "PV maximum power-point tracking by using artificial neural network," *Mathematical Problems in Engineering*, vol. 2012, Article ID e506709, 10 pages, 2012.

[26] J. de Dieu Nguimfack-Ndongmo, B. P. Ngoussandou, D. Goron et al., "Nonlinear neuro-adaptive MPPT controller and voltage stabilization of PV systems under real environmental conditions," *Energy Reports*, vol. 8, pp. 1037–1052, 2022.

[27] N. Rajasekar, M. Vysakh, H. V. Thakur et al., "Application of Modified Particle Swarm Optimization for Maximum Power Point Tracking under Partial Shading Condition," *Energy Procedia*, vol. 61, pp. 2633–2639, 2014.

[28] S. Mohanty, B. Subudhi, and P. K. Ray, "A new MPPT design using Grey wolf optimization technique for photovoltaic system under partial shading conditions," *IEEE Transactions on Sustainable Energy*, vol. 7, no. 1, pp. 181–188, 2016.

[29] S. Titri, C. Larbes, K. Y. Toumi, and K. Benatchba, "A new MPPT controller based on the ant colony optimization algorithm for photovoltaic systems under partial shading conditions," *Applied Soft Computing*, vol. 58, pp. 465–479, 2017.

[30] N. Kumar, B. Singh, and B. K. Panigrahi, "Integration of solar PV with low-voltage weak grid system: using maximize-M Kalman filter and self-tuned P&O algorithm," *IEEE Transactions on Industrial Electronics*, vol. 66, no. 11, pp. 9013–9022, 2019.

[31] N. Kumar, B. Singh, and B. K. Panigrahi, "LLMLF-based control approach and LPO MPPT technique for improving performance of a multifunctional three-phase two-stage grid integrated PV system," *IEEE Transactions on Sustainable Energy*, vol. 11, no. 1, pp. 371–380, 2020.

[32] N. Kumar, B. Singh, B. K. Panigrahi, C. Chakraborty, H. M. Suryawanshi, and V. Verma, "Integration of solar PV with low-voltage weak grid system: using normalized Laplacian kernel adaptive Kalman filter and learning based InC algorithm," *IEEE Transactions on Power Electronics*, vol. 34, no. 11, pp. 10746–10758, 2019.

[33] N. Kumar, B. Singh, B. K. Panigrahi, and L. Xu, "Leaky-least-logarithmic-absolute-difference-based control algorithm and learning-based InC MPPT technique for grid-integrated PV system," *IEEE Transactions on Industrial Electronics*, vol. 66, no. 11, pp. 9003–9012, 2019.

[34] N. Kumar, B. Singh, J. Wang, and B. K. Panigrahi, "A framework of L-HC and AM-MKF for accurate harmonic supportive control schemes," *IEEE Transactions on Circuits and Systems I: Regular Papers*, vol. 67, no. 12, pp. 5246–5256, 2020.

[35] N. Femia, *Power Electronics and Control Techniques for Maximum Energy Harvesting in Photovoltaic Systems*, Crc Press, Taylor & Francis Group, 2013.

[36] W. Xiao and W. G. Dunford, "A modified adaptive hill climbing mppt method for photovoltaic power systems," in *2004 IEEE 35th Annual Power Electronics Specialists Conference (IEEE Cat. No.04CH37551)*, pp. 1957–1963, Aachen, Germany, 2004.

[37] Q. Mei, M. Shan, L. Liu, and J. M. Guerrero, "A novel improved variable step-size incremental-resistance mppt method for pv systems," *IEEE Transactions on Industrial Electronics*, vol. 58, no. 6, pp. 2427–2434, 2011.

[38] Y. Jiang, J. A. Qahouq, and T. A. Haskew, "Adaptive step size with adaptive-perturbation-frequency digital mppt controller for a single-sensor photovoltaic solar system," *IEEE Transactions on Power Electronics*, vol. 28, no. 7, pp. 3195–3205, 2013.

[39] S. Jain and V. Agarwal, "A new algorithm for rapid tracking of approximate maximum power point in photovoltaic systems," *IEEE Power Electronics Letters*, vol. 2, no. 1, pp. 16–19, 2004.

[40] A. Ali, K. Almutairi, S. Padmanaban et al., "Investigation of MPPT techniques under uniform and non-uniform solar irradiation condition–a retrospection," *IEEE Access*, vol. 8, pp. 127368–127392, 2020.

[41] M. Killi and S. Samanta, "Modified perturb and observe MPPT algorithm for drift avoidance in photovoltaic systems," *IEEE*

Transactions on Industrial Electronics, vol. 62, no. 9, pp. 5549–5559, 2015.

[42] A. F. Tchouani Njomo, L. L. Sonfack, R. M. Douanla, and G. Kenne, "Nonlinear neuro-adaptive control for MPPT applied to photovoltaic systems," *Journal of Control, Automation and Electrical Systems*, vol. 32, no. 3, pp. 693–702, 2021.

[43] S. J. Moura and Y. A. Chang, "Lyapunov-based switched extremum seeking for photovoltaic power maximization," *Control Engineering Practice*, vol. 21, no. 7, pp. 971–980, 2013.

[44] G. Masters, *Renewable and Efficient Electric Power Systems*, Wiley Online. Library, 2004.

[45] G. Vachtsevanos and K. Kalaitzakis, "A hybrid photovoltaic simulator for utility interactive studies," *IEEE Transactions on Energy Conversion*, vol. EC-2, no. 2, pp. 227–231, 1987.

[46] M. G. Villalva, J. R. Gazoli, and E. R. Filho, "Comprehensive approach to modeling and simulation of photovoltaic arrays," *IEEE Transactions on Power Electronics*, vol. 24, no. 5, pp. 1198–1208, 2009.

[47] W. De Soto, S. A. Klein, and W. A. Beckman, "Improvement and validation of a model for photovoltaic array performance," *Solar Energy*, vol. 80, no. 1, pp. 78–88, 2006.

[48] H. Tian, F. Mancilla-David, K. Ellis, E. Muljadi, and P. Jenkins, "A cell-to-module-to-array detailed model for photovoltaic panels," *Solar Energy*, vol. 86, no. 9, pp. 2695–2706, 2012.

[49] A. F. Tchouani Njomo, G. Kenne, R. M. Douanla, and L. L. Sonfack, "A modified ESC algorithm for MPPT applied to a photovoltaic system under varying environmental conditions," *International Journal of Photoenergy*, vol. 2020, Article ID 1956410, 15 pages, 2020.

[50] D. Baimel, S. Tapuchi, Y. Levron, and J. Belikov, "Improved fractional open circuit voltage MPPT methods for PV systems," *Electronics*, vol. 8, no. 3, p. 321, 2019.

[51] A. Chellakhi, S. El Beid, and Y. Abouelmahjoub, "Implementation of a novel MPPT tactic for PV system applications on MATLAB/Simulink and Proteus-based Arduino board environments," *International Journal of Photoenergy*, vol. 2021, Article ID 6657627, 19 pages, 2021.

[52] V. J. Chin, Z. Salam, and K. Ishaque, "An improved method to estimate the parameters of the single diode model of photovoltaic module using differential evolution," in *2015 4th international conference on electric power and energy conversion systems (EPECS)*, Sharjah, United Arab Emirates, 2015.

[53] A. Chellakhi, S. El Beid, and Y. Abouelmahjoub, "An innovative fast-converging speed MPPT approach without oscillation for temperature varying in photovoltaic systems applications," *Energy Sources, Part A: Recovery, Utilization, and Environmental Effects*, vol. 44, no. 2, pp. 2674–2696, 2022.

[54] I. Khan and S. Khan, "Thermal imaging based maximum power point tracking for solar modules in variable ambient temperature," *Applied Sciences*, vol. 3, no. 5, pp. 1–10, 2021.

[55] Y. Wang, Y. Yang, G. Fang et al., "An advanced maximum power point tracking method for photovoltaic systems by using variable universe fuzzy logic control considering temperature variability," *Electronics*, vol. 7, no. 12, p. 355, 2018.

[56] P. K. Pathak, A. K. Yadav, and P. A. Alvi, "Reduced oscillations based perturb and observe solar maximum power point tracking scheme to enhance efficacy and speed of a photovoltaic system," *Journal of Engineering Research*, pp. 1–13, 2022.

[57] K. Saidi, M. Maamoun, and M. H. Bounekhla, "A New High Performance Variable Step Size Perturb-And-Observe MPPT Algorithm for Photovoltaic System," *International Journal of Power Electronics and Drive Systems (IJPEDS)*, vol. 10, no. 3, p. 1662, 2019.

[58] X. Li, H. Wen, L. Jiang, W. Xiao, Y. du, and C. Zhao, "An improved MPPT method for PV system with fast-converging speed and zero oscillation," *IEEE Transactions on Industry Applications*, vol. 52, no. 6, pp. 5051–5064, 2016.

[59] J. Ahmed and Z. Salam, "An improved perturb and observe (P&O) maximum power point tracking (MPPT) algorithm for higher efficiency," *Applied Energy*, vol. 150, pp. 97–108, 2015.

[60] M. Hebchi, A. Kouzou, and A. Choucha, "A modified variable step size for Maximum Power Point tracking based on Perturb and observe algorithm," *Electrotehnica, Electronica, Automatica (EEA)*, vol. 66, no. 4, pp. 1582–5175, 2018.

[61] I. Owusu-Nyarko, M. A. Elgenedy, I. Abdelsalam, and K. H. Ahmed, "Modified variable step-size incremental conductance MPPT technique for photovoltaic systems," *Electronics*, vol. 10, no. 19, p. 2331, 2021.

[62] F. Liu, S. Duan, F. Liu, B. Liu, and Y. Kang, "A variable step size INC MPPT method for PV systems," *IEEE Transactions on Industrial Electronics*, vol. 55, pp. 2622–2628, 2008.

[63] N. N. E. Zakzouk, M. A. Elsaharty, A. K. Abdelsalam, A. A. Helal, and B. W. Williams, "Improved performance low-cost incremental conductance PV MPPT technique," *IET Renewable Power Generation*, vol. 10, no. 4, pp. 561–574, 2016.

[64] L. Yang, Z. Yunbo, L. Shengzhu, and Z. Hong, "Photovoltaic array MPPT based on improved variable step-size incremental conductance algorithm," in *Proceedings of the 2017 29th Chinese control and decision conference (CCDC)*, Chongqing, China, May 2017.

[65] R. Faraji, A. Rouholamini, H. R. Naji, R. Fadaeinedjad, and M. R. Chavoshian, "FPGA-based real time incremental conductance maximum power point tracking controller for photovoltaic systems," *IET Power Electron*, vol. 7, no. 5, pp. 1294–1304, 2014.

[66] M. A. Gomes de Brito, L. Galotto Jr., L. P. Sampaio, G. e Melo, and C. A. Canesin, "Evaluation of the main MPPT techniques for photovoltaic applications," *IEEE Transactions on Industrial Electronics*, vol. 60, no. 3, pp. 1156–1167, 2013.

[67] A. Al Nabulsi and R. Dhaouadi, "Efficiency optimization of a DSP-based standalone PV system using fuzzy logic and dual-MPPT control," *IEEE Transactions on Industrial Informatics*, vol. 8, no. 3, pp. 573–584, 2012.

[68] M. A. Zainuri, M. A. Radzi, A. Che Soh, and N. A. Rahim, "Development of adaptive perturb and observe-fuzzy control maximum power point tracking for photovoltaic boost dc–dc converter," *IET Renewable Power Generation*, vol. 8, no. 2, pp. 183–194, 2014.

[69] P. C. Sekhar and S. Mishra, "Takagi–Sugeno fuzzy-based incremental conductance algorithm for maximum power point tracking of a photovoltaic generating system," *IET Renewable Power Generation*, vol. 8, no. 8, pp. 900–914, 2014.

[70] Y. Jiang, J. Abu Qahouq, and T. Haskew, "Adaptive-step-size with adaptive-perturbation-frequency digital MPPT controller for a single-sensor photovoltaic solar system," *IEEE transactions on power Electronics*, vol. 28, no. 99, pp. 3195–3205, 2011.